

Influence of volatile fatty acids on aerobic granular sludge performance and considerations for pre-fermentation

by

Lindsey Carver

in partial fulfillment of the requirements for the degree
Master of Science in Civil Engineering
at the Delft University of Technology

November 2020

Thesis committee: Prof. Dr. M. de Kreuk, TU Delft, Chair
Prof. Dr. J. van Lier, TU Delft
Ir. E. van Dijk, RHDHV
Dr. M. Pronk, TU Delft, RHDHV



Confidentiality of this Report

This study was commissioned by Royal HaskoningDHV. No part of this report may be reproduced and/or published by print, photocopy, microfilm or by any other means, without the prior written permission of HaskoningDHV Nederland B.V.; nor may any part of the report be used, without such permission, for any purposes other than that for which it was produced.

Abstract

Pre-fermentation of influent has been proposed as a method to improve phosphorus removal capacity, granulation, and simultaneous nitrification denitrification for aerobic granular sludge plants. This thesis sought to determine the influence of increasing VFA concentrations on performance of aerobic granular sludge plants and key considerations for implementation of pre-fermentation. Two approaches were applied during this thesis: a modelling approach and an experimental approach. A mathematical model was built to show the influence of increasing VFA concentrations and to describe principles observed in practice at aerobic granular sludge plants. The experimental approach consisted of two measuring campaigns. First, experiments were performed to test the necessary operational conditions to ferment influent in a sequencing batch reactor fermenter. Second, a sampling campaign was conducted to determine the conditions which led to fermentation of organic matter in a sand trap on site in Utrecht. The model demonstrated the benefit of combining existing models to describe settling of aerobic granular sludge with size fractionations, plug flow feeding in a settled sludge bed, reactions in the bulk and in granules, and diffusion across granules and into bulk liquid. It was found that increasing acetate concentrations led to longer stability of phosphorus uptake capacity and that SRT control is necessary to maintain long term capacity. Increasing acetate concentrations also led to increases in phosphate release and simultaneous nitrification denitrification. These changes were attributable to differences observed across granules of different sizes: phosphate accumulating organisms dominated larger granules and nitrifiers were more dominant in smaller granules. Model calculations indicate that a maximum granule size exists because the most poly-phosphate storage was not performed by the largest granules. From the experimental work, fermentation was found to be occurring (at rates of $21 \text{ mg VFA-COD L}^{-1} \text{ h}^{-1} \pm 15$) in a hydraulically underloaded sand trap which led to significant VFA production and subsequent difficulties in fermenting in the controlled SBR reactor (which produced an average of 28 mg VFA-COD/l). More research is needed to determine the optimal operational conditions to ferment influent and to demonstrate the effect on aerobic granular sludge in practice.

Contents

Abstract	2
List of Figures.....	5
List of Tables.....	5
List of Acronyms	6
Acknowledgements	7
1. Introduction and literature review.....	8
1.1 Introduction.....	8
1.1.1 COVID-19	9
1.1.2 Problem statement and research questions.....	9
1.2 Literature review	10
1.2.1 Wastewater complexity and aerobic granular sludge.....	10
1.2.2 Mathematical modeling of aerobic granular sludge	11
1.2.3 Fermentation and influent characteristics	12
1.2.4 Pre-fermentation for EBPR.....	13
2. Methodology	13
2.1 Mathematical modeling	13
2.1.1 Building blocks.....	13
2.1.2 Single granule diameter model	15
2.1.3 Simulations.....	16
2.1.4 Influent characteristics and model parameters	17
2.1.5 Assumptions and modifications	17
2.2 Fermentation experiments.....	18
2.2.1 Fermentation SBR.....	18
2.2.2 Fermentation batch tests	19
2.2.3 Lab analysis.....	20
2.2.4 Online measurements	20
3. Results: Modeling.....	21
4. Results: Pre-fermentation	29
5. Discussion	33
5.1 Limitations of the single granule diameter model	33
5.2 Different population shifts in different granule sizes	33
5.3 Lack of total nitrogen removal	34
5.4 Nutrient conversion rates.....	35
5.5 Consumption of acetate by different species & the unique role of different granule sizes	35
5.6 Loss of phosphate uptake capacity without SRT control	36

5.7 Stability of phosphate uptake capacity with higher acetate concentrations.....	36
5.8 Influence of exchange ratios on AGS performance.....	37
5.9 Model limitations	37
5.10 Implications of fermentation observed in the sand trap	38
5.11 Limitations of studying sand trap fermentation	38
5.12 Unstable performance in fermenter	39
5.13 Connection between high fermentation in sand trap and low fermentation in fermenter	39
5.14 Possible other factors for unstable fermenter performance.....	39
5.15 Different fermentative activity observed in biomass across the PNU	40
6. Conclusions.....	41
7. Recommendations.....	42
References.....	43
Appendix A: Model matrices & parameters.....	47
Appendix B: Single granule model.....	51
Appendix C: Concentration profiles over granules, end of feeding	52
Appendix D: PP storage per granule size over time	55
Appendix E: VFA production rate vs. peak concentrations in PNU	57
Appendix F: Additional sand trap measurements	60
Appendix G: Biomass activity and microscopy.....	61
Appendix H: VFA production rates in the sand trap over time	64
Appendix I: Oxygen penetration over different granule sizes	65
Appendix J: Substrate front vs. sludge bed expansion.....	68

List of Figures

Figure 1: Nereda® phases.....	8
Figure 2: Schematic of anaerobic degradation pathways	12
Figure 3: Granule profile for 2.2 mm granule	16
Figure 4: Configuration of PNU	18
Figure 5: 28.6-L fermenter	18
Figure 6: Averaged reactor bulk concentrations.....	22
Figure 7: Bulk concentrations over time	24
Figure 8: Average concentrations across the granule radius	26
Figure 9: Average PHA storage over per granule size	26
Figure 10: Poly-phosphate storage per granule size.....	27
Figure 11: PHA storage per granule size.....	28
Figure 12: VFA production rate in fermenter over time	29
Figure 13: VFA measured in three locations in the PNU primary treatment during a feeding phase ..	30
Figure 14: Eight-hour batch test: VFA production rate per biomass sample	31
Figure 15: Variation in VFAs over the sand trap depth	31

List of Tables

Table 1: Pre-fermentation of domestic wastewater	13
Table 2: Model parameters and influent characteristics	17
Table 3: Fermenter operational settings and phase schedule	19
Table 4: Average nutrient conversion rates during the stable removal phase ii	25
Table 5: Fermenter measurements – average VFA & MLSS.....	29
Table 6: COD and VS of influent before and after sand trap.....	30

List of Acronyms

Acronym	Definition
AGS	aerobic granular sludge
AOB	ammonium oxidizing bacteria
ASM	activated sludge model
BAP	biochemical acidogenic potential
COD	chemical oxygen demand
DO	dissolved oxygen
EBPR	enhanced biological phosphorus removal
EGSB	expanded granular sludge bed
EPS	extracellular polymeric substance
GAO	glycogen accumulating organisms
HRT	hydraulic retention time
HUSB	hydrolytic upflow sludge blanket
IFAS	integrated fixed-film activated sludge
MBBR	moving bed biofilm reactor
MLSS	mixed liquor suspended solids
NOB	nitrite oxidizing bacteria
OHO	ordinary heterotrophic organisms
PAO	phosphorus accumulating organisms
PHA	polyhydroxyalkanoate
PID	proportional integral derivative
SBR	sequencing batch reactor
SND	simultaneous nitrification denitrification
SRT	solids retention time
TS	total solids
TSS	total suspended solids
UASB	upflow anaerobic sludge blanket
VFA	volatile fatty acids
VS	volatile solids
VSS	volatile suspended solids
WWTP	wastewater treatment plant

Acknowledgements

This thesis would not be here if it weren't for the help and support of many people.

Firstly, I'd like to thank my supervisors at RHDHV: Edward van Dijk, Mario Pronk, and Pascale Vermeulen, thank you for all the time and energy you put into helping me with this project. I appreciate the knowledge you shared with me, the insights you gave, and the ease of conversation. Especially with the transition to working from home, it was a pleasure to have such an energetic team to work with.

I would also like to thank my committee members: Merle de Kreuk and Jules van Lier, thank you for your unique perspectives and input. You have inspired me to do my best.

Many thanks to Sara Toja Ortega for your input from the beginning, especially with the practical work, I would have been lost in the lab without your help. Viktor Haaksman, you were extremely patient and helpful guiding me through the ever-evolving model. Jelle Langedijk, thank you for all the help building and troubleshooting in Utrecht. Thanks to you, Mark Stevens, and Pascale for the wonderful company and assistance on site. Thanks to those who consulted with me from RHDHV and the Sanitary Engineering Department at TU Delft.

Finally, I'd like to thank my friends and family for joining me on this journey. Especially to Casper van der Stelt for being there for the rambling moments of doubt and the celebrations alike.

1. Introduction and literature review

1.1 Introduction

Aerobic granular sludge (AGS) is a biological treatment technology proven to efficiently remove nutrients from wastewater. The concept of aerobic granular sludge was first reported in the 1990s (Morgenroth et al., 1997), (Heijnen and van Loosdrecht, 1998), (Beun et al., 1999), (Dangcong et al., 1999) and has been studied extensively since then. This technology was developed further at TU Delft and was marketed as Nereda® by Royal HaskoningDHV. There are now more than 60 aerobic granular sludge plants in operation. This technology is operated in a sequencing batch reactor (SBR) with granular sludge which has very high settling rates (de Kreuk et al., 2007a), (van Dijk et al., 2020a). Because of this, no clarifiers are needed and there is a short settling period in the SBR, allowing for reactor volumes to remain small (De Bruin et al., 2004). The phases employed in the Nereda® process can be seen in Figure 1.

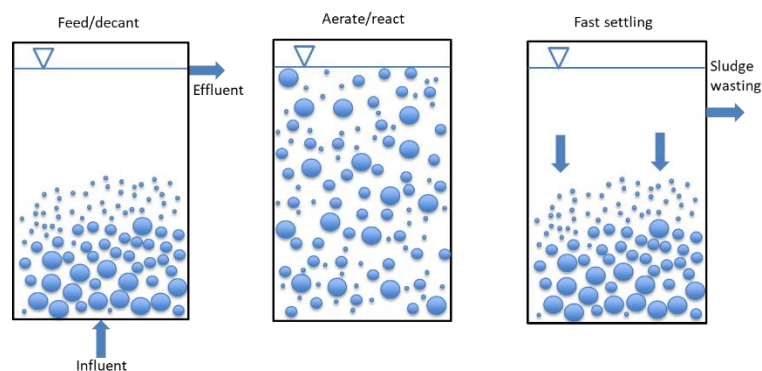


Figure 1: Nereda® phases

Due to the varied penetration of substrates and oxygen into the granule, different biological activity occurs at the surface of the granule than in the center (de Kreuk, et al., 2007b). This allows the granules to perform nitrogen and phosphorus removal in a smaller, single compartment reactor compared to typical enhanced biological phosphorus removal (EBPR) systems.

AGS plants are operated to select for phosphorus accumulating organisms (PAOs) which dominate the granule population (de Kreuk et al., 2007a). During the feeding phase, PAOs hydrolyze poly-phosphate and glycogen to give energy for the uptake of volatile fatty acids (VFAs) which are stored as polyhydroxyalkanoates (PHA) (Metcalf et al., 1979). This occurs during anaerobic conditions and causes phosphate to be released into the water. During aerobic conditions, PAOs then grow on the stored PHA and simultaneously uptake phosphate from the water to replenish the poly-phosphate stores in the cell. This leads to a net removal of phosphate from the wastewater. In some operating AGS plants, biological phosphorus removal is not always sufficient to meet regulations. Iron dosing is commonly applied in these scenarios to meet regulations, which drives operational costs up.

Initial lab scale research into AGS was performed using synthetic wastewater, commonly with feed with chemical oxygen demand (COD) in the form of VFAs (Beun et al., 2001) (de Kreuk et al., 2007b). This readily available form of substrate led to quick granule formation at the lab scale. Additionally, wastewaters with high VFA concentrations, such as some industrial wastewaters, frequently experience faster startup (faster formation of a mature granular bed) and more stable operation than those with low VFA concentrations, such as domestic wastewater (de Kreuk & van Loosdrecht, 2006). PAOs require approximately 20 mg VFA-COD/l to remove 1 mg/l of phosphorus (Smolders, G.J.F., 1995). Because of this, it is expected that additional conversion of readily biodegradable COD (rbCOD) to VFAs is needed to consistently meet regulations in AGS plants that must currently dose iron. Several

domestic plants must include an anoxic phase after aeration to denitrify because the amount of simultaneous nitrification denitrification (SND) is low (Pronk et al., 2015b). This is due to the ratio of rbCOD/N which is less favorable in low loaded full-scale systems. rbCOD is produced from hydrolysis of slowly degradable COD during aeration (Pronk et al., 2015a). While control systems to improve SND are available (van Dijk et al., 2020b), the rates are limited by hydrolysis. Pre-fermentation of influent has been proposed as a method to remedy these problems through conversion of rbCOD to VFAs, increasing availability of acetate during anaerobic feeding for improved EBPR and SND.

It is suspected that increased loading of volatile fatty acids in wastewater can lead to increased phosphorus uptake capacity and simultaneous nitrification denitrification. Redesign of AGS influent buffer tanks for pre-fermentation has been proposed to increase VFA loading to AGS plants. This thesis explored what the impact of pre-fermentation of influent would be on AGS performance and the conditions necessary to achieve fermentation in a buffer tank. An AGS model was developed to determine the impact of increased VFA loading on performance and experiments were performed to better identify the conditions necessary to ferment domestic influent in a buffer tank.

Granulation rate is also influenced by the VFA concentrations in influent. Uptake of VFAs (available from influent and through fermentation of rbCOD) in the anaerobic feeding phase is needed to grow PAOs preferentially over ordinary heterotrophic organisms (OHOs) (Haaksman et al., 2020) and maintaining PAO competition over OHOs is necessary to maintain granules with high settling velocities. Therefore, increases in VFA concentrations could lead to shorter startup time and could possibly eliminate the need for seeding reactors with granular sludge, leading to cost savings.

1.1.1 COVID-19

Due to COVID-19, unexpected time constraints for experimental work occurred. The fermenter was designed, built, and startup was initiated, however, process optimization was not possible before the COVID-19 crisis began. At this point, COVID-19 regulations did not allow for experiments to proceed. In the meantime, the focus of this thesis shifted to modeling. After the first lockdown, the reactor was started up again. However, there was not enough time left for extensive troubleshooting. Investigations into the primary treatment system on site (at the prototype Nereda® in Utrecht) led to new insights. These insights both showed potential for fermentation in a different manner and revealed likely causes of unstable fermenter performance.

1.1.2 Problem statement and research questions

The purpose of this research was to gain insight into the operation of a pre-fermenter designed for AGS and to anticipate what the influence of pre-fermentation would be on AGS performance. The focus of the experimental research was on identification of the key conditions to ferment influent in a buffer tank. Modification of operational conditions and the specific sewage composition are also very important factors to consider in future research, but these were not within the scope of this thesis. Modeling is used to estimate the effect of a range of influent VFAs on performance. The range of VFAs modeled in the influent was based on the VFA concentrations observed in the experimental phase. The modeling gives an indication of how impactful pre-fermentation potentially is and if it is realistic to implement at existing or planned AGS plants. The combined results can be used as an indicator of the necessary pre-fermenter volume and operational parameters. This thesis sought to answer the following question:

What is the influence of increasing VFAs on aerobic granular sludge performance and what are key mechanisms for fermentation of domestic wastewater?

The overarching research question can be elaborated with the following subquestions:

1. What is the influence of pre-fermentation on phosphorus removal capacity?

It was expected that higher concentrations of acetate in the influent would improve the phosphorus removal capacity. Large granules settle faster and are, therefore, present at the bottom of the sludge blanket and will receive the most substrate from the influent. Higher concentrations of VFA will allow for smaller granules to take up VFAs as well. Increased PHA storage across all granules could allow for more phosphorus removal over time.

2. What is the influence of pre-fermentation on nutrient conversion rates?

It was expected that the amount of phosphate release, phosphate uptake, and simultaneous nitrification denitrification would increase. This is because more acetate will lead to more PHA storage in the granules. Release and uptake of phosphate is related to PHA storage and SND is improved when more PHA storage is available in the anoxic zones of the granules.

3. What is the role of different granule sizes in nutrient removal?

It was expected that larger granules would contain relatively more PAOs than smaller granules. Inert cores were expected to be larger with increasing granule size due to diffusion limitations. This could mean that there is an optimal maximum granule size for efficient phosphate removal. Additionally, with low VFA concentrations, nitrifier concentrations were expected to be relatively higher in smaller granules due to reduced competition with PAOs (because of less PHA storage during feeding) and due to better penetration of oxygen and ammonium across the entire granule depth. This would mean that small granules are necessary to nitrify while large granules are necessary for phosphate removal and simultaneous nitrification denitrification.

4. What is the fate and role of VFAs in an AGS system?

It was expected that VFAs would be taken up primarily by larger granules due to their presence at the bottom of the sludge bed. It was expected that this effect would be more prominent when batch sizes are reduced because there will be less contact between smaller granules and substrate in the influent during feeding. VFAs are expected to be primarily stored as PHA in the PAOs anaerobically and then used for growth of PAO and storage of poly-phosphate aerobically.

5. What VFA production rates are achieved in a pre-fermentation buffer tank and which variables are critical for stable fermentation?

It was expected that up to $19 \text{ mg VFA g TSS}^{-1} \text{ hr}^{-1}$ could be produced through fermentation of influent (González-Barceló et al., 2006). It was expected that biomass which could be separated from the influent through settling would be formed and that an 8-hour hydraulic retention time (HRT) was sufficient to ferment domestic influent at 20°C .

This report will detail the literature review, applied methodology, modeling results, experimental results, discussion, and then conclusions.

1.2 Literature review

1.2.1 Wastewater complexity and aerobic granular sludge

As previously described, VFAs are converted to storage polymers by PAOs under anaerobic conditions. These storage polymers act as carbon donors for nutrient removal under aerobic conditions. Domestic wastewater is typically composed of a mixture of particulate and readily biodegradable substrates in addition to low concentrations of VFAs (Henze et al., 2008). While it is expected that hydrolysis and fermentation of influent COD leading to production of VFAs is performed by granules and flocs during

the anaerobic phase, the extent of this has not yet been quantified (Wagner et al., 2015). The quantity of available VFAs in full scale plants during the anaerobic feeding phase or during aeration is therefore unclear.

Different influent characteristics have been seen to lead to different granule characteristics, start-up times, and performance. It has been observed that faster granulation and better settleability occurs with feed composed of rapidly diffusible substrates (de Kreuk et al., 2007a) (Pronk et al., 2015a). Maintaining preferential conditions for slower growing PAOs over ordinary heterotrophs (OHOs) is critical for maintaining stability of the AGS process. Layer et al. (2019) found that complex influent led to fermenters outcompeting PAOs, however, this does not match the experiences from practice (Pronk et al., 2015b). Haaksman et al. (2020) found that maintaining anaerobic uptake of rbCOD was key to maintaining the competitive advantage of PAOs over OHOs.

AGS performance is also influenced by the complexity of substrate in the feed as this impacts the availability of the carbon source for denitrification and phosphorus removal (Morgenroth et al., 2002). Differences in the diffusion rate of soluble substrates influence where carbon sources are available in a granule and the fate of particulates is, until now, unclear (Wagner et al., 2015). Soluble substrates diffuse into the granules and VFAs are stored as PHA. The size of the granules influences how deep these carbon sources are available, which in turn influences the amount of simultaneous nitrification denitrification (de Kreuk et al., 2010). Deeper penetration of VFAs allows for PHA available in the anoxic zone of the granules for denitrification. PAOs can also consume VFAs aerobically, therefore, acetate which has yet been consumed anaerobically or rbCOD which is fermented in the granule can still be taken up. It has been observed that starch is adsorbed to the granules, hydrolyzed, and then substrate could diffuse into the granule. It is expected that other particulate substrates in domestic wastewater similarly do not diffuse into the granules (Carlson & Silverstein, 1998) and that flocculent biomass is largely responsible for conversion of particulates due to higher surface area. However, the mechanisms behind hydrolysis of particulates in AGS systems are difficult to determine and are not yet clear.

The use of influent pre-fermentation to increase VFA concentrations has recently been proposed for application in AGS plants (Yuan et al., 2020). The use of pre-fermentation with glucose feed has been explored, however, complex influent has not yet been utilized. Despite the lack of research on the topic, designs have already been proposed with pre-fermentation buffer tanks. This is a research area that needs to be addressed.

1.2.2 Mathematical modeling of aerobic granular sludge

Mathematical models are commonly applied to explore research questions which are difficult or very time-consuming to perform experimentally, especially considering the long SRT for AGS reactors. Aerobic granular sludge has been described with many models (Beun et al., 2001) (Su & Yu, 2006) (de Kreuk et al., 2007b) (Winkler et al., 2015) (Dold et al., 2018) (Baeten et al., 2018). In these models, a 1-D biofilm approach is commonly used where the spherical granules are discretized into concentric layers from the core outward. Reactions within each granule layer are calculated using Monod kinetics and diffusion equations are used to find the transfer of substrates across the granule layers and into the bulk liquid. Diffusion is driven by the concentration gradients between the outer granule layer and the bulk liquid as well as those present between the granule layers. Reactions are commonly described with activated sludge models (ASM) which have been found to accurately describe lab-scale granular reactors.

Despite the numerous available models, there are still gaps between the behaviors that models describe and observations from practice. It is suspected that this is related to several factors. Few models have attempted to describe a reactor with multiple granule sizes. Additionally, the effect of

plug flow feeding into a settled sludge bed has not been explored. This was expected to have a large influence due to the variable availability of substrate over the sludge bed. Plug flow feeding also induces higher concentration gradients between the liquid and granules than would occur in a mixed feeding phase. Many models have been used to describe conditions at lab scale, typically with high acetate concentrations. As lab scale models do not include the separation of different forms of influent COD, these models cannot accurately predict the behavior of full-scale plants which receive influent with a large proportion of particulate COD. Layer et al. (2020) modeled AGS to compare lab scale conditions with full scale conditions through inclusion of particulate COD, readily degradable COD, and VFAs. However, this model utilized a mixed bulk liquid and did not successfully include adaptations for plug flow and settling. Because of this, the variability in storage polymers for granules spread over the sludge bed could not be captured.

This thesis sought to bridge these modeling gaps in addition to exploring the influence of increasing VFA concentrations in domestic wastewater to gauge the extent to which pre-fermentation improves AGS performance.

1.2.3 Fermentation and influent characteristics

The ideal conditions for hydrolysis and fermentation of influent have been identified for application to anaerobic wastewater treatment technologies such as upflow anaerobic sludge blanket (UASB) and expanded granular sludge bed (EGSB). The influent characteristics themselves alter the process as different pathways are followed for proteins, carbohydrates, and lipids. A general schematic for anaerobic digestion can be seen in Figure 2.

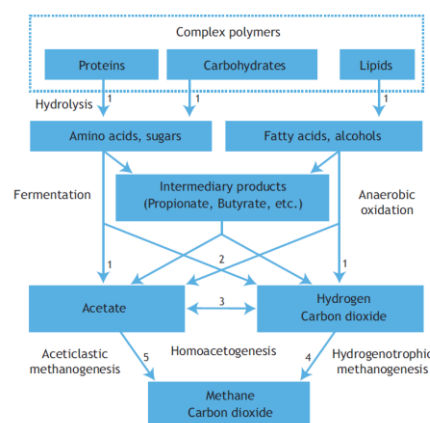


Figure 2: Schematic of anaerobic degradation pathways , adopted from (Henze et al., 2008)

In order to optimize VFA production, hydrolysis and acidogenesis must be optimized and methanogenesis must be inhibited. Hydrolysis is most commonly the rate limiting step for digestion of domestic wastewater (Henze et al., 2008). For ease of analysis and comparison of different wastewater treatment plants, the COD of influent is typically divided into the following categories: inert, slowly biodegradable, fermentable, and readily available (VFAs) (Henze et al., 2000).

To ferment domestic wastewater, the two primary parameters that need to be controlled to perform specific anaerobic conversions are solids retention time and contact between the sludge and the wastewater (Henze et al., 2008). Several operational parameters are also important for achieving fermentation such as temperature and pH. Literature indicates that an SRT ranging from 2 to 8 days at ambient temperatures will lead to fermentation of domestic wastewater without favoring the growth of methanogenic bacteria (Miron et al., 2000) (Danesh & Oleszkiewicz, 1997) (Bouzas et al., 2007). The largest increase in fermentation was seen when the SRT was increased from 0 to 3 days. Fermentation

proceeds with HRTs from 2.5 to 10 hours at temperatures from 14 to 26°C (Yuan et al., 2011) (Metcalf et al., 1979). Different configurations have been tested to separate the SRT and HRT to perform fermentation with smaller reactor sizes such as sequencing batch reactors (SBRs), hydrolytic upflow sludge beds (HUSBs), and activated primary clarifiers (APC). Psychrophilic temperatures have also been seen to lead to fermentation in full scale installations (Münch & Koch, 1999).

1.2.4 Pre-fermentation for EBPR

The topic of fermentation of raw influent and primary sludge has been explored extensively in regards to optimizing enhanced biological phosphorus removal (EBPR) (Nicholls et al., 1985) (Abu-Ghararah & Randall, 1991) (Münch & Koch, 1999). Table 1 shows a review of technologies which have been investigated for influent fermentation and production of VFAs for EBPR processes. Due to the batch cycles used with AGS, a buffer tank is commonly used to regulate the flows. Several technologies investigated for fermentation of influent for EBPR could be applied in a buffer tank configuration for AGS plants.

Table 1: Pre-fermentation of domestic wastewater, configurations from literature and VFA production rates

Configuration	Inf. COD (mg/l)	Org. Loading (kg COD m ⁻³ d ⁻¹)	HRT (hrs)	SRT (days)	Temp (C)	VFA production rates
SBR (González-Barceló et al., 2006)	-	0.62-0.72	8	2-8	22 - 31	633 g VFA m ⁻³ d ⁻¹ 449 mg VFA g TSS ⁻¹ d ⁻¹
HUSB (Ligero et al., 2001)	525- 710		2.2-4.4		20	426-884 g VFA m ⁻³ d ⁻¹ 36.2-74 mg VFA g VSS ⁻¹ d ⁻¹
HUSB (Alvarez et al., 2003)	360- 470	1.2 - 3.9	2.9-7.1	10-50	16-20	237-513 g VFA m ⁻³ d ⁻¹ 23.2-74.4 mg VFA g VSS ⁻¹ d ⁻¹
HUSB (Alvarez et al., 2008)	100- 500	0.5-3.2	2.8-5.7	28.8	14-21	16-534 g VFA m ⁻³ d ⁻¹ 1.4-44.6 mg VFA g VSS ⁻¹ d ⁻¹

2. Methodology

2.1 Mathematical modeling

2.1.1 Building blocks

Several models are available for different parts of the AGS process, but to be able to model the fate of VFAs in an AGS reactor, an integrated approach was necessary. In the ongoing PhD projects of Haaksman and van Dijk, such a model has been developed. However, this model lacked an extensive description of biological conversions. In this thesis, this model was extended to include these reactions according to the ASM2d model (Henze et al., 2000) with corrections by Hauduc et al. (2010), both in the biofilm and the bulk liquid. This model was built in Python and later optimized with the use of Numba. The model was composed of three key components to describe flow, settling, and reaction/diffusion, as detailed below.

Flow model

The plug flow feeding in the reactor was simulated with an axial dispersion model as described by Degaleesan and Dudukovic (1998) with an added convection term (van Dijk et al., 2018).

$$\frac{dc}{dt} = D_{ax} \frac{d^2c}{dx^2} + v \frac{dc}{dx} \quad (1)$$

As described in van Dijk et al. (2018), c is the concentration in the bulk liquid, D_{ax} is a coefficient which includes turbulent dispersion and convection, x is reactor depth, and v is the liquid upflow velocity.

Settling model

To determine which granules receive VFAs and which granules do not, the distribution of granules in the reactor must be described. This was done with the settling model adapted from the Richardson and Zaki model (Richardson and Zaki, 1954). The adapted model, as described by van Dijk et al. (2020a), included the settling of individual granules. Hereto the apparent voidage fraction (ε_{ei}) was used to convert individual granules to bulk behavior:

$$\varepsilon_{ei} = 1 - \left[1 + \left(\frac{d_{avg}}{d_i} \right) \left[(1 - \varepsilon)^{-\frac{1}{3}} - 1 \right] \right]^3 \quad (2)$$

Where d_{avg} is the average diameter of all granules, d_i is the diameter of a granule size fraction, and ε is the voidage of the reactor.

Since this model was based on an adapted version of the Richardson and Zaki model, this model could accurately describe the settling behavior of the granules, as well as the fluidization and segregation of granules in the settling phase.

Reaction model

The reaction model had two parts: the reaction in the granule and the reaction in the bulk liquid. For the former, a reaction/diffusion model was used, based on a Crank Nicolson (Crank and Nicolson, 1947) discretization of Fick's law, including a reaction term. For the reaction term, the ASM2d matrix was added to the model. For ease of modification of model parameters, the matrix and parameters were maintained in an Excel document, as built by Schroeten, I. (2019). Since in this model, individual granules (representing granules of a similar size) were described, every granule had its own state of components of the ASM2d model.

For the bulk liquid, the ASM2d model was added as a reaction term. Coupling between the bulk liquid and the biofilm was done by describing the external mass transfer.

$$-D_i \left. \frac{\partial C_{s,i}}{\partial x} \right|_{x=LS} = k_{i,SL} (C_{L,i} - C_{S,i}) \quad (3)$$

Where D_i is the diffusion coefficient for each solute, i , x is the depth of the boundary layer, $C_{S,i}$ is the concentration of the solute in the outermost layer of the granule, $C_{L,i}$ is the concentration in the bulk liquid. $k_{i,SL}$ (in m/s) was determined based on a correlation with the Sherwood number.

$$k_{i,SL} = \frac{Sh \cdot D}{d} \quad (4)$$

The Sherwood number was determined by considering two possible porosities: that similar to a complete packing or medium packing bed.

In Fan et al. (1960), a complete packing bed (around 50% porosity) is described with a Sherwood number:

$$Sh = 2 + 1.51 * ((1 - \varepsilon) * Re)^{\frac{1}{2}} * Sc^{\frac{1}{3}} \quad (5)$$

In Cussler, E. L., (2009), a medium packing bed (around 80% porosity) is described with a Sherwood number:

$$Sh = 2 + 0.6 * (Re_c)^{\frac{1}{2}} * Sc^{\frac{1}{3}} \quad (6)$$

The included symbols are as follows:

ε : voidage (-)

Re: particle Reynolds number, $Re = \rho v d_p / \mu$

Re_c : particle Reynolds number corrected using local liquid velocity around granule, $Re = \rho v_p d_p / \mu$

Sc: Schmidt number, $Sc = (\mu/\rho)/D$

v: empty column superficial velocity (m/s)

v_p : local liquid velocity around the particle (m/s)

μ : dynamic viscosity (Pa*s)

ρ : displaced liquid density (kg/m³)

D: diffusion coefficient of chemical (m²/s)

In this model, only solutes could diffuse into the granule, therefore particulates could only be converted in the bulk reactions. Flocculent biomass could be included in the bulk for these conversions; however, this was not applied for the described scenarios. This can be included in the future. Growth of granules was not included; the initial diameter was kept constant. To see the effect of changes in species in the granule, a redistribution was applied.

Changes in biomass populations in the granules

Several models which described the growth of granules have found that the biomass populations are not stable until 200 to 800 days have passed (de Kreuk et al., 2007b) (Winkler et al., 2015). These periods are significantly longer than the SRT of 30 days which is typically applied to AGS plants (Ali et al., 2019). This shows that a steady state for granule populations is likely never achieved in practice. Because this thesis aimed to identify the short-term effect of different VFA concentrations on granules, growth was not included. Granule sizes were set to be constant in the model. The summed concentration of particulates within the granule were maintained at a constant concentration: 50 kg TSS/m³. Each time step, the distribution of the biomass and particulates in the granule were redistributed after growth and decay such that the total TSS concentrations and granule size were constant over time. The starting distribution of species and storage polymers was determined after reaching stable conditions in the simplified model.

After each time step, the re-distribution for all species, i, was calculated for each layer of each granule.

$$X_{i,t+1} := \frac{X_{i,t+1}}{\sum_{i=0}^N X_{i,t+1}} * \sum_{i=0}^N X_{i,t} \quad (7)$$

2.1.2 Single granule diameter model

Because this model was developed concurrently with the ongoing PhD work of Haaksman and van Dijk, initially, a model was developed which described the behavior of one granule size (single granule model). This model did not include the flow or settling models; therefore, a uniform mixed bulk liquid was used for all phases. The goal of this model was to identify a reasonable species distribution across the granule to implement in the multi-granule model. This model also allowed for testing of the implementation of ASM2d kinetics in the framework which was under development for the PhD work of Haaksman and van Dijk. The simplifications also allowed for long runs to be performed quickly to

reach semi-steady state conditions. This simplified model described the reactions and diffusion into granules of only one size (2.2 mm diameter). In this model, settling and plug flow feeding into a settled bed were not yet incorporated therefore the reactor bulk liquid was equivalently mixed during all phases.

In this model, 8 g TSS/l of granules (with a diameter of 2.2 mm) were included in a lab scale reactor of 3 L volume. Granule growth was not implemented, rather redistribution of species within each granule layer was implemented (as described in the methods). An exchange ratio of 40% was applied with the following influent concentrations: 400 mg/l acetate, 80 mg/l rbCOD, 45 mg/l ammonium, and 8 mg/l phosphate. A one hour feeding phase was used where concentrations were increased incrementally for six minutes (to avoid large concentration gradients to maintain stable diffusion). The aerobic phase was controlled with proportional integral derivative (PID) controller with a dissolved oxygen (DO) setpoint of 1 mg/l and k_{la} of 3 hr^{-1} . The length of aeration was controlled with a stopping setpoint of 4 mg/l ammonium.

The single granule diameter model was run under these conditions until steady state conditions were reached. The bulk concentrations over time and the steady state cycle for this model can be found in Appendix B. Figure 3 shows the steady state distribution of species and storage polymers over the granule radius.

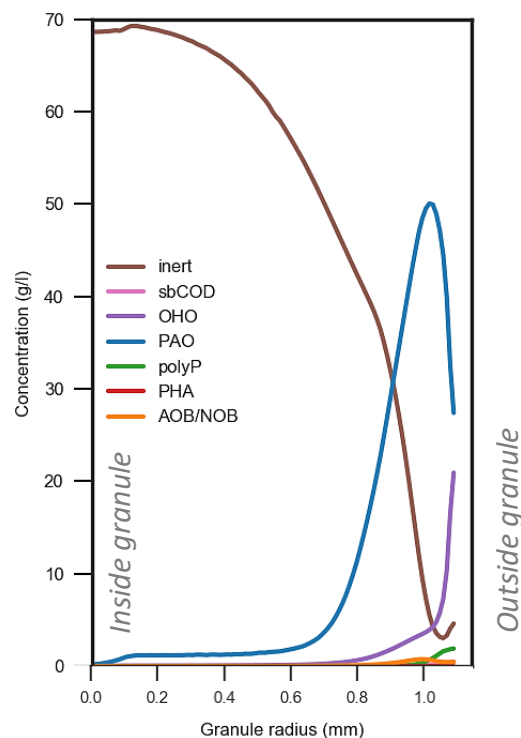


Figure 3: Granule profile for 2.2 mm granule during steady state conditions with influent concentrations: 400 mg/l acetate, 80 mg/l rbCOD, 45 mg NH_4/l , 8 mg P/l, 40% exchange ratio, and 8 g TSS/l.

These distributions were obtained after correcting for mathematical errors in the profiles (original profiles can be seen in Appendix B). Linear interpolation was used to replace outlier values in the curves. This corrected steady state granule profile was used to define the initial conditions across the granules for the multi-granule model. For the multi-granule model, the same profile was applied for all granule sizes.

2.1.3 Simulations

Two different simulations were run for the multi-granule model. Pre-fermentation was simulated through increasing acetate concentrations (and equivalently reducing rbCOD concentrations) for 50,

100, and 150 mg VFA-COD/l. Additionally, the effect of varying the exchange ratio was simulated through reducing the batch size from 50%, 25%, and 12.5%. In the exchange ratio simulations, the upflow velocity was the only parameter changed to achieve the different batch sizes. The influent concentrations were constant; therefore, the loading was reduced. The feeding time was kept constant at one hour and 100 mg VFA-COD/l was used. One additional simulation was performed by adjusting the exchange ratio to 25% by shortening the anaerobic feeding time and maintaining the same upflow velocity. For the exchange ratio runs, it was necessary to set nitrate concentrations to zero at the end of each cycle to avoid significant amounts of pre-denitrification within the granule volumes with low VFA loads and low SND.

2.1.4 Influent characteristics and model parameters

The influent COD fractionation in wastewater can vary at different wastewater treatment plants and is not commonly measured. The COD fractionation as detailed in Henze et al. (2008) was used assuming a total COD of 600 mg/l (see Table 2). Readily biodegradable COD is typically around 20% of the total COD and acetate was set according to a range found in practice (and the rbCOD was altered respectively). The key model and influent characteristics used for each simulation can be found in Table 2.

Table 2: Model parameters and influent characteristics

*three runs with varying VFA concentrations and rbCOD were performed with a 50% exchange ratio

**distribution from reactor 4 in Utrecht WWTP on 3/10/2019 (concentrations are ordered respective to the listed diameters)

***three runs with varying exchange ratios were performed with constant influent characteristics (using 100 mg/l acetate)

Multi-granule model	
Influent VFA (mg COD/l)	50, 100, 150*
Influent rbCOD (mg COD/l)	117, 67, 17*
Influent NH ₄ (mg N/l)	60
Influent PO ₄ (mg P/l)	10
Reactor height (m)	1.5
Reactor volume (l)	3
Granule diameters (mm)	0.21, 0.51, 0.8, 1.2, 1.7, 2
Biomass concentration (g TSS/l)	0.67, 0.27, 0.5, 1.06, 2.03, 1.47**
Exchange ratio	0.5, 0.25, 0.125***
DO setpoint (mg/l)	2.0
K _{la} (hr ⁻¹)	10
dt (s)	1
Feed phase (hrs)	1
NH ₄ setpoint for end of aeration phase (mg/l)	1

A list of all model parameters can be found in Appendix A.

2.1.5 Assumptions and modifications

The following modifications were applied to ASM2d kinetics:

- PAO decay factor was reduced to 0.05 as it has been found to be significantly lower in practice (Lu et al., 2007)
- PAO decay only occurred aerobically. This was based on research which showed negligible decay of PAOs under anaerobic and anoxic conditions (Lu et al., 2007).
- PAO and heterotroph limitations on ammonium and phosphate were removed. This is because the model did not include organic sorbed ammonium or phosphate. In full scale plants, ammonium and phosphate are not limiting for PAO or heterotrophs. This is due to the presence of sorbed nutrients in extracellular polymeric substances (EPS). Literature has shown that bacteria adapt EPS to store additional nutrients when limitations would otherwise occur.

- A maximum ratio of 0.5 g PHA/g PAO was set in the granules. Although the maximum may be different, this assumption was used to avoid unrealistic concentrations of PHA in the granules.

The complete description of the kinetics used for the model can be found in Appendix A.

2.2 Fermentation experiments

To better understand how to apply pre-fermentation in the context of an AGS plant, an anaerobic SBR tank was operated and monitored from June - October 2020. This will be referred to as the fermenter. The fermenter was fed influent from a prototype AGS system. Due to difficulties with startup of the fermenter, analysis was performed on the treatment scheme prior to the fermenter. It was determined that fermentation was primarily occurring in the grit removal tank and buffer tank prior to the intake point for the fermenter. The details of the configuration can be seen in Figure 4.

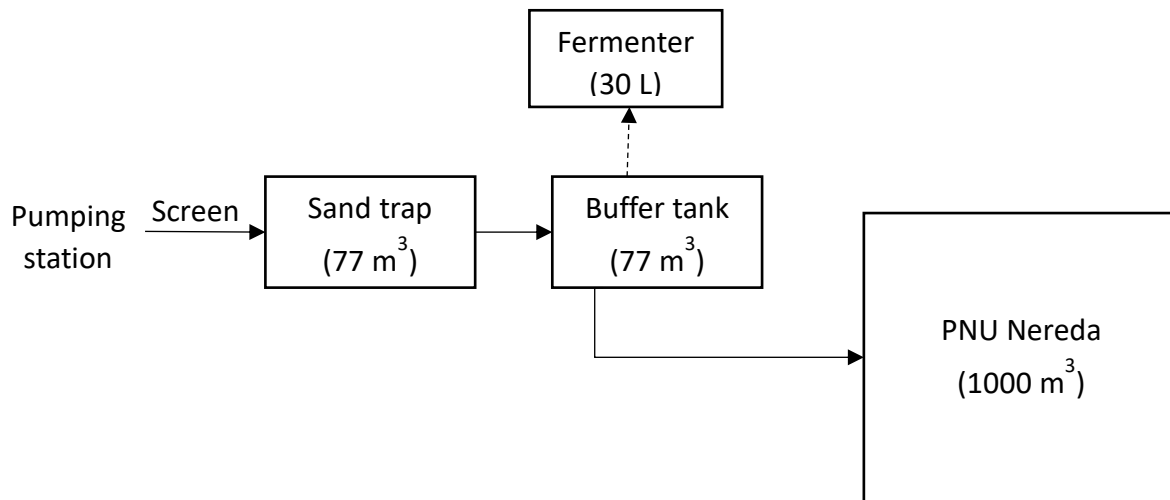


Figure 4: Configuration of PNU

2.2.1 Fermentation SBR

A 28.6-L automated fermenter was designed and then built from PVC as shown in Figure 5.



Figure 5: 28.6-L fermenter

The fermenter was located at the Utrecht WWTP at a prototype Nereda[®], henceforth referred to as the PNU. The PNU receives influent from the Utrecht region. The influent passes through rotating screens, a sand trap, and then a buffer tank before entering the Nereda[®] tank.

The sand trap and buffer tank are each 77 m³. The horizontal velocity through the sand trap during this period was 0.02-0.03 m/s. This is ten times lower than the typical design criteria for grit removal (Metcalf et al., 1979). This system is used for research purposes and the configuration in use led to this unintended hydraulically underloaded state. The PNU is 1000 m³ and has a loading rate of 0.08 kg COD kg MLSS⁻¹ d⁻¹.

The fermenter received influent pumped from the buffer tank with a hose pump with a pumping rate of 1 L/m. An exchange ratio of 0.45 was used (13 liters of influent were added per cycle). An aquarium heater was used to maintain a temperature of 20°C. Additionally, a shade cloth was installed to minimize solar influence on the temperature. During the reaction phase, the reactor was mixed with an impeller with two blades attached to a 65 rpm DOGA motor. A settling phase is then performed with no mixing and a selection pressure of 1.5 m/h was used. An electrical ball valve (JP Fluid Control) is opened to decant the supernatant (13 liters per cycle). The fermenter cycles were controlled with a Raspberry Pi. The phase schedule and settings can be seen in Table 3. Two phases were defined with HRTs as shown below. Additionally, during phase 2, the fermenter feeding phase occurred while influent was flowing to the PNU during feeding.

Table 3: Fermenter operational settings and phase schedule

	Phase 1	Phase 2
HRT (hours)	8	16
Feed	13 min	13 min
React	7 hrs, 32 min	7 hrs, 32 min
Settle	12 min	12 min
Discharge	3 min	3 min
SRT (d)	1.6 ± 0.4	7.9 ± 3.1
Temperature (deg C)	20.9 ± 3.4	21.3 ± 5.8

In addition to manual sampling from the fermenter, manual samples were collected from the pumping station, grit removal tank, and buffer tank. Automatic samples were taken from the buffer tank based on time (instead of preferably flow) to form daily composite samples. The intake for these samples was located on the far end of the buffer tank while the fermenter received influent pumped from the middle of the buffer tank.

2.2.2 Fermentation batch tests

To determine the fermentation activity of the biomass present in the system, batch tests were performed. A modified biochemical acidogenic potential (BAP) test was performed following the protocol described in Ruel et al. (2002). The redox of each bottle was checked to ensure anaerobic conditions in place of sparging nitrogen gas. As the goal of the test was to determine the difference in fermentation activity, biomass was added to each bottle. Raw influent collected from the pumping station for the PNU was fermented by biomass from the fermenter, settled sludge from the grit removal tank, and biofilm from the walls of the grit removal tank. Because the expected increase in VFAs was small (per the rates observed in the fermenter), it was desirable to minimize VFA production on products of biomass degradation itself. Therefore, the volume of added biomass was such that the total COD from the biomass was lower than the total COD from the influent. Additionally, controls were performed using the influent and each of the biomass samples separately.

2.2.3 Lab analysis

Samples were filtered directly through a 0.45 μm filter for VFA analysis with Hach LCK365 kits for indicative results. Additional filtered sample was immediately frozen and final analysis was performed with gas chromatography (GC). For GC analysis, pentanol was added as an internal standard and the sample was acidified with formic acid. Total COD and soluble COD (after filtration through paper filters of 47 μm) was measured with Hach LCK514 kits. TS, TSS, and VS were measured on fresh samples following standard procedures (Association et al., 1915).

2.2.4 Online measurements

The fermenter was fitted with a temperature probe, pH probe (Atlas Scientific), and level sensor. These were placed in the top half of the reactor and measured continuously. A Hach online VFA analyzer (EZ7250) was installed to sample from the PNU buffer tank in September. This analyzer sampled from a continuous fast loop which circulated influent from the PNU buffer tank at a speed of 3 m^3/h .

3. Results: Modeling

Modeling was performed to determine the influence of pre-fermentation on aerobic granular sludge performance and to identify the key principles involved. The multi-granule model was used to show the effect of short-term changes caused by pre-fermentation of influent. The results of this model are detailed in this section.

The multi-granule model includes granules of different diameters, the settling model, and the plug flow feeding model. The multi-granule model was used to compare the effect of different concentrations of influent acetate and rbCOD to simulate the effect of pre-fermentation of readily biodegradable COD on the phosphate and nitrogen conversions. The model used granule diameters of 0.21, 0.51, 0.8, 1.2, 1.7, and 2 mm with concentrations of 0.67, 0.27, 0.5, 1.06, 2.03, and 1.47 g TSS/l respectively (distribution from reactor 4 in Utrecht on 3/10/2019). The initial species distribution for all granules was based on the steady state profiles found for the single granule diameter model (from Figure 3). The concentration of each species per granule volume was kept constant by interpolating the concentrations across the granule layers based on the percent depth into the radius (as described in the methods).

Three runs were performed, with all settings kept constant except the influent acetate and rbCOD concentrations. The acetate concentrations were 50, 100 and 150 mg/l and the corresponding rbCOD concentrations were 117, 67, and 17 mg/l. The detailed model parameters for all runs can be seen in Appendix A. This results section will first detail the changes observed in a cycle with stable nutrient removal and then show the changes in the performance over time. Finally, details about the differences observed in granules of different sizes will be shown.

For all runs, an exchange ratio of 50% was used with influent characteristics: 600 mg total COD/l, 60 mg ammonium/l, and 10 mg phosphate/l. In the graphs of reactor bulk concentrations through all the phases, the bulk concentration is displayed as an average over the reactor. This is accurate due to mixing during aeration. However, the concentrations shown in the graph during feeding are not representative of the concentrations which were modeled to be in contact with granules during anaerobic plug-flow feeding. In full scale systems, the collected data will show ammonium and phosphate peaks after mixing begins due to sampling from the top of the reactor.

Each of the runs went through a period of initialization where nutrient removal capacity was increased, stable conversions of ammonium and phosphate, and then a deterioration of phosphate conversion processes. These periods will be described in more detail later. Firstly, an example of the cycles with stable removal with different influent acetate concentrations can be seen in Figure 6.

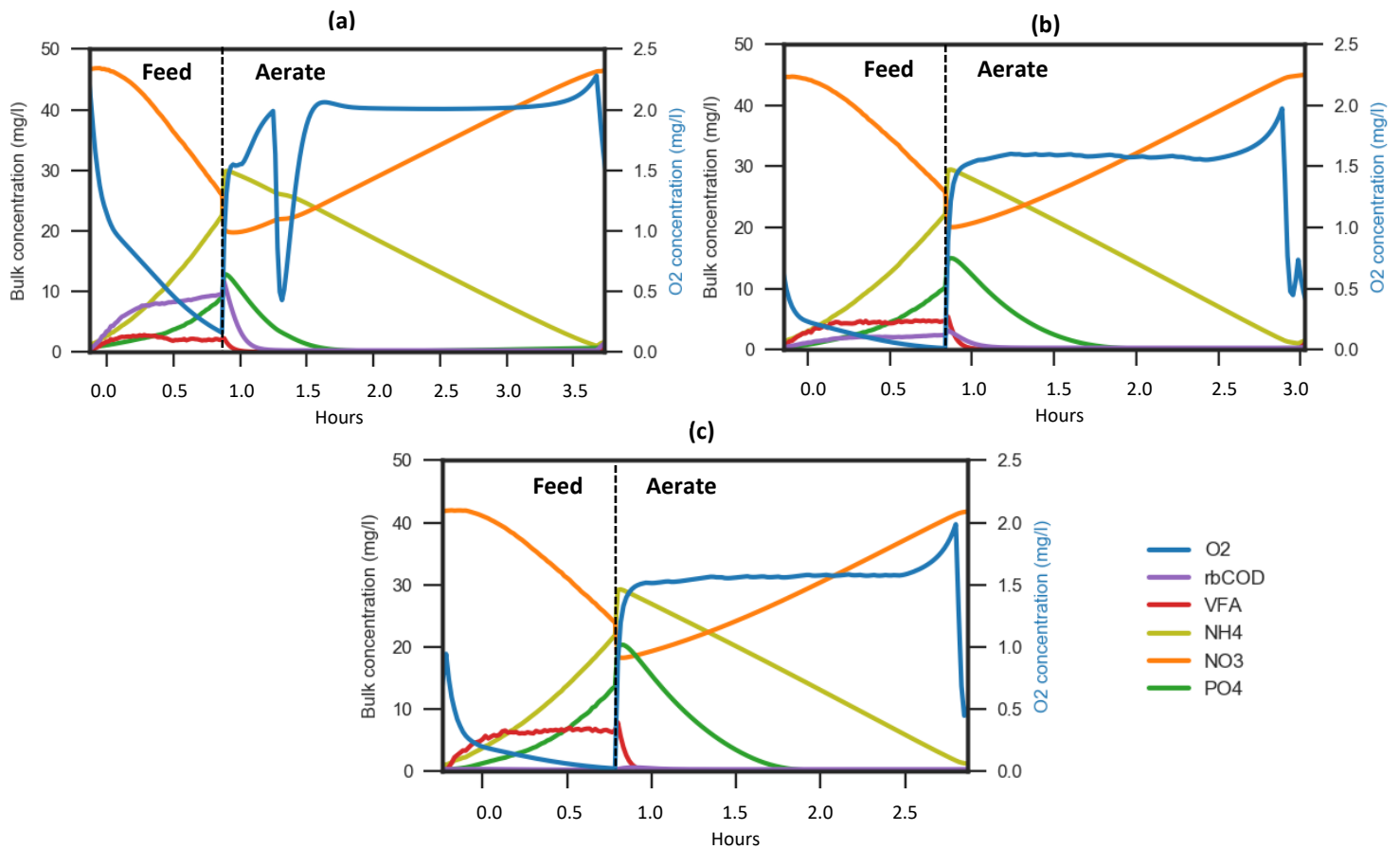


Figure 6: Averaged reactor bulk concentrations over a cycle during the stable conversion phase. (a) 50 mg/l acetate, (b) 100 mg/l acetate, (c) 150 mg/l acetate. Oxygen concentrations are indicated on the right axis (O₂) while all other concentrations are on the left axis (bulk). 50% exchange ratio is used with influent characteristics: 600 mg tCOD/l, 60 mg NH₄/l, 10 mg PO₄/l. Modeled granule sizes: 0.21, 0.51, 0.8, 1.2, 1.7, and 2 mm with respective concentrations: 0.67, 0.27, 0.5, 1.06, 2.03, and 1.47 g TSS/l. Note that during plug flow feeding, average concentrations over the reactor are displayed although concentrations vary over the reactor depth.

The cycle began with plug flow feeding through a settled granule bed and decant from the top of the reactor (as shown in Figure 1). During feeding, ammonium and phosphate increased as influent was fed. Phosphate also increased due to the release of poly-phosphate stores from PAOs anaerobically to provide energy to store acetate as PHA. Because of the plug flow feeding, effluent with remaining nitrate and oxygen from the previous cycle was discharged while the influent remained anaerobic. Denitrification during an anoxic phase was not included in the model, therefore, nitrate concentrations were higher than typically seen in practice. At the end of feeding, in every run, there was a small amount of remaining acetate and/or readily biodegradable COD in the bulk. Once aeration began, acetate and readily biodegradable COD was consumed preferentially by heterotrophs. This affected the competition between heterotrophs and PAOs. In the ASM2d kinetics, PAOs can take up acetate aerobically.

During aeration, oxygen concentrations were controlled with a PID controller. The PID controller increased the oxygen added to the system by both considering the difference between the DO setpoint and the current oxygen concentrations in the liquid and the history of how much oxygen was added.

Because of this effect, jumps in the oxygen concentrations sometimes occurred (as occurs in Figure 6a).

The applied oxygen transfer coefficient (k_{la}) was high (10 hr^{-1}) so the DO setpoint of 2 mg/l was reached almost immediately. Phosphorus was taken up aerobically by PAOs and growth of PAOs occurred under aerobic conditions. Additionally, nitrifiers converted ammonium to nitrate under aerobic conditions. Depending on the availability of PHA in deeper anoxic zones in the granules, simultaneous denitrification could be performed during aeration. The length of the aerobic phase was determined with a stopping setpoint of 1 mg/l of ammonium. Once this setpoint was reached, the aeration stopped and settling occurred. The cycle then began again. No wasting was performed because of the method applied to maintain constant biomass concentrations (as described in the methods section).

As mentioned previously, the runs went through three stages: initialization, stable removal, and deterioration of removal processes. All runs started with identical initializations in the granules (from the single granule model) which had too few autotrophs to perform complete nitrification. This led to ammonium in the effluent during phase i. Therefore, all runs began with an increase in autotrophic populations to develop sufficient ammonium removal capacity (initialization). Ammonium oxidizing bacteria (AOB) and nitrite oxidizing bacteria (NOB) were not modeled separately in ASM2d kinetics. Nitrification was therefore simplified as a one-step process as ammonium converted directly to nitrate in the model. Stable nutrient removal profiles were reached, within 4-5 days of operation (equivalent to within 30 cycles). The progression of the cycles can be seen in Figure 7 for each of the runs. The stable removal period was characterized by the complete removal of ammonium and phosphate (effluent quality showed less than 1 mg/l for both). In the final phase, phosphate removal capacity declines, and effluent concentrations exceeded 1 mg/l.

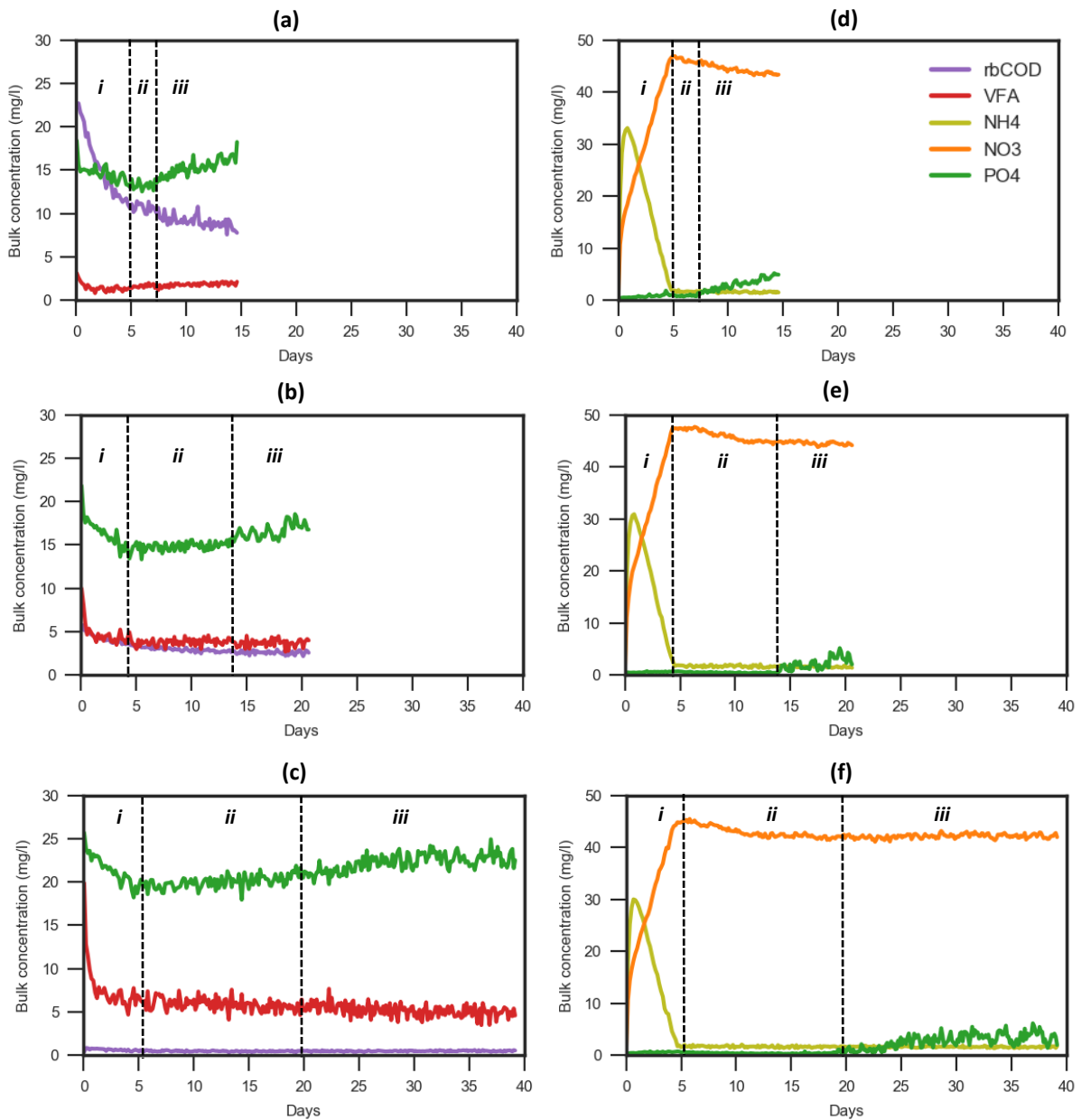


Figure 7: Bulk concentrations over time at the end of feeding (left) and in the effluent (right), (a, d) 50 mg/l acetate, (b, e) 100 mg/l acetate, (c, f) 150 mg/l acetate. The rbCOD, acetate, and phosphate concentrations at the end of feeding are seen in (a), (b), and (c) while the effluent concentrations of ammonium, nitrate, and phosphate are seen in (d), (e), and (f). The division between the 3 phases (*i*=initialization, *ii*=stable removal, and *iii*=deterioration of removal) are marked with dashed lines.

Figure 7a-c show that at the end of feeding, the acetate and rbCOD were not completely consumed. This allowed for COD to be consumed aerobically, preferentially by heterotrophs in the system.

The loss of phosphorus removal capacity in all runs can be seen in the effluent phosphate concentrations for each cycle shown in Figure 7d-f. The run lengths were varied to capture this behavior. For the model run with 50 mg/l of acetate, within 8 days of operation (around 50 cycles), the phosphate effluent concentrations exceeded the threshold of 1 mg/l. With 100 mg/l and 150 mg/l acetate it took around 15 and 23 days respectively for the same increase in effluent concentrations to begin in the model. The variability in each cycle for all parameters was due to the stochastic nature of the model. Granule positioning was randomized during aeration which causes the settled sludge bed

to form with different granules at the bottom for each cycle. If a small granule was located at the bottom of the reactor at the end of the aeration phase, it remained at the bottom. Thereby received more substrate during feeding than the average small granule which was located at the top of the sludge bed due to slower settling rates. This random process was hypothesized to occur in practice. Therefore, the phosphate release and subsequent effluent quality showed some variability even during the stable removal period.

The average rates observed in the runs during stable removal can be seen in Table 4. The rates were all calculated based on the changes observed in the reactor bulk liquid. While ammonium and phosphate are both also removed for growth of biomass, this was not separated in the rate calculations.

Table 4: Average nutrient conversion rates during the stable removal phase ii

Rates	50 mg/l acetate	100 mg/l acetate	150 mg/l acetate
Ammonium removal (mgL ⁻¹ hr ⁻¹)	11.4	12.9	13.4
Simultaneous denitrification (mgL ⁻¹ hr ⁻¹)	0.9	1.5	2.1
Phosphate release (mgL ⁻¹ hr ⁻¹)	12.3	14.0	19.6
Phosphate uptake (mgL ⁻¹ hr ⁻¹)	16.1	18.4	18.2

As acetate concentrations increased, ammonium removal, simultaneous nitrification denitrification, and phosphate release rates all increased.

Figure 8 shows the distribution of species and storage polymers across the radius of granules of different sizes (small (0.21 mm diameter), medium (0.8 mm), and large (2 mm) granules) during the stable period for the run with 150 mg/l of acetate.

The concentration profiles when 50 and 100 mg/l of acetate were applied can be found in Appendix C (with all granule sizes included). Similar profiles across different granule sizes were observed at all acetate concentrations, although more heterotrophs and fewer autotrophs were present with increasing rbCOD concentrations. The displayed profiles are at the end of the aeration phase.

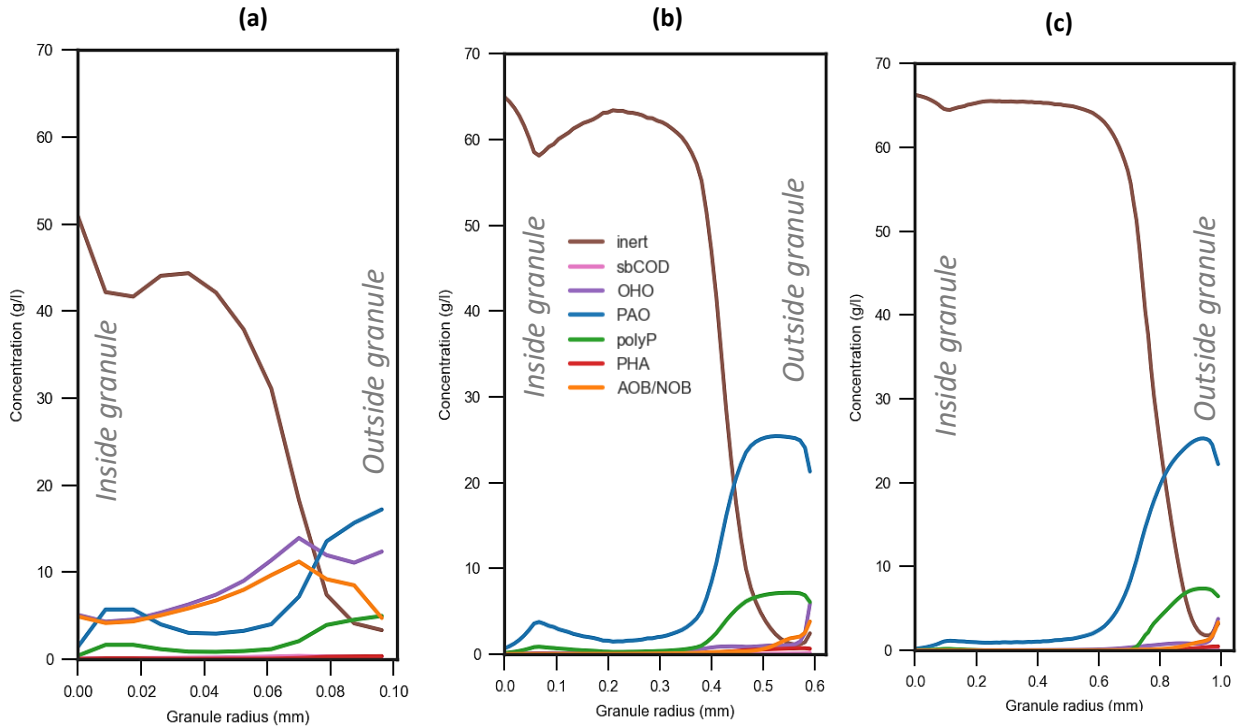


Figure 8: Average concentrations across the granule radius for each size fraction once stable removal is reached, using 150 mg/l acetate in the influent where (a) is 0.2 mm granule, (b) is 0.8 mm granule, and (c) is 2 mm granule

The distributions reflect the average of all the granules with the selected radius. The figures from left to right show the smallest (0.21 mm), middle (0.8 mm), and largest (2 mm) granule size. The profiles for granules of 0.5, 1.2, and 1.7 mm diameter can be found in Appendix C. It can be observed that all granules contained a primarily inert core (brown line). The larger granules were, the larger the inert core was, and the active layer shifted toward the outer layers. The largest concentration of PAOs in the granule could be found in the medium sized granules while the largest concentrations of autotrophs and heterotrophs were found in the smallest granules. In all granules and in all runs, the PHA was completely depleted at the end of the aeration phase.

The difference in species across granules was related to the availability of substrate over the settled sludge bed during anaerobic feeding. This can be seen through the variability in PHA storage for granules of different sizes. Figure 9 shows the PHA stored in each granule size fraction in total during each cycle.

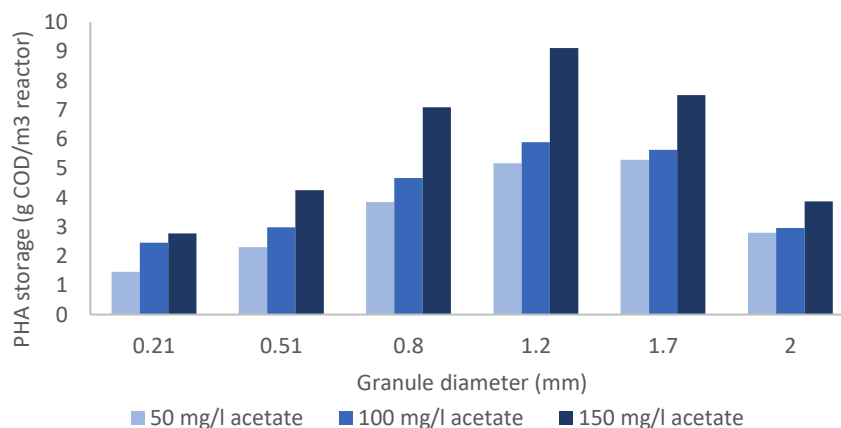


Figure 9: Average PHA storage over per granule size (g COD/m³ reactor), for each granule size and run with increasing VFA concentrations

Granules of 1.2 mm diameter stored the most PHA in the reactor, followed by 1.7 and 0.8 mm diameter granules.

Figure 10 shows the contribution of each granule size fraction to uptake of phosphate in the reactor. These figures are all from the run with 100 mg/l acetate. In these figures the accumulation of poly-phosphate over time (because there is no SRT control) in the granules can be seen. The figures for 50 m/l and 150 mg/l acetate can be found to show similar trends in Appendix D.

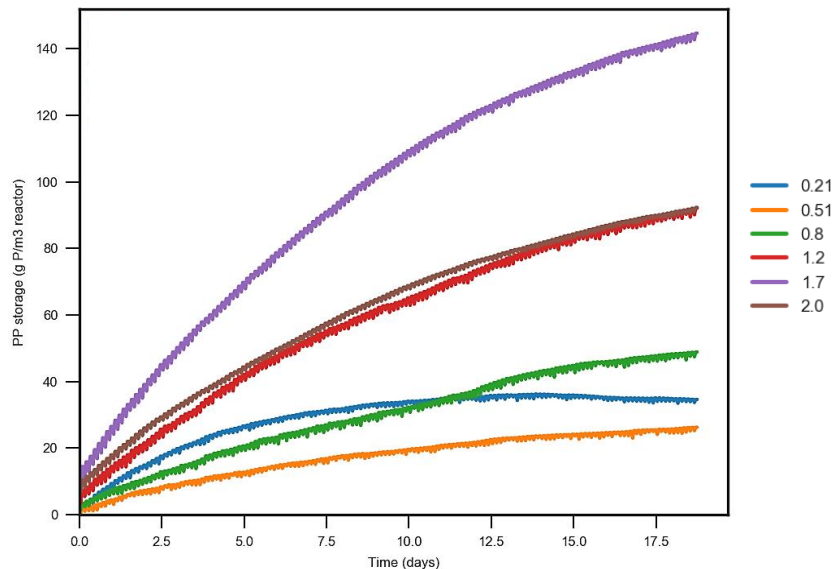


Figure 10: Poly-phosphate storage per granule size, total contribution of each granule size fraction to phosphate removal in the reactor (g P/m³ granule) in terms of poly-phosphate storage over time.

From Figure 10, it can be seen that the granules of 1.7 mm performed the most uptake of phosphate from the bulk and that granules of 2 and 1.2 mm take up the next largest amount. In all cases, the uptake of phosphate could be seen to decrease over time as the granules approached the point of poly-phosphate storage saturation.

The second set of simulations pertained to the influence of exchange ratios. When the exchange ratio simulations were run, the distribution of PHA storage over the granule sizes changed. As the exchange ratio increased from 12.5% to 25% to 50% (though altering the upflow velocity but keeping the anaerobic feeding time and influent concentrations the same), the average penetration of the substrate front into the sludge bed increased from 42% to 59% to 95% respectively (examples of these runs can be seen in Appendix J). The effect of this on the PHA storage can be seen in Figure 11.

When the exchange ratio increased, the distribution of acetate over the sludge bed became more even. When the exchange ratio was small, the PHA storage for the granule of 1.7 mm diameter was more prominently the largest. Additionally, exchange ratios influenced the percent of the acetate from the influent which was stored as PHA versus being used by other organisms. By summing the stored PHA for all granule sizes, the total PHA storage in the reactor could be calculated. This was compared with the total acetate loading. In the 12.5% exchange ratio, 94% of the loaded acetate was stored as PHA while 89% and 93% resulted for 25% and 50% exchange ratios respectively. When the exchange ratio was achieved through a shorter feeding time the storage per acetate loading was only 74% and the substrate penetration into the sludge bed was 68%.

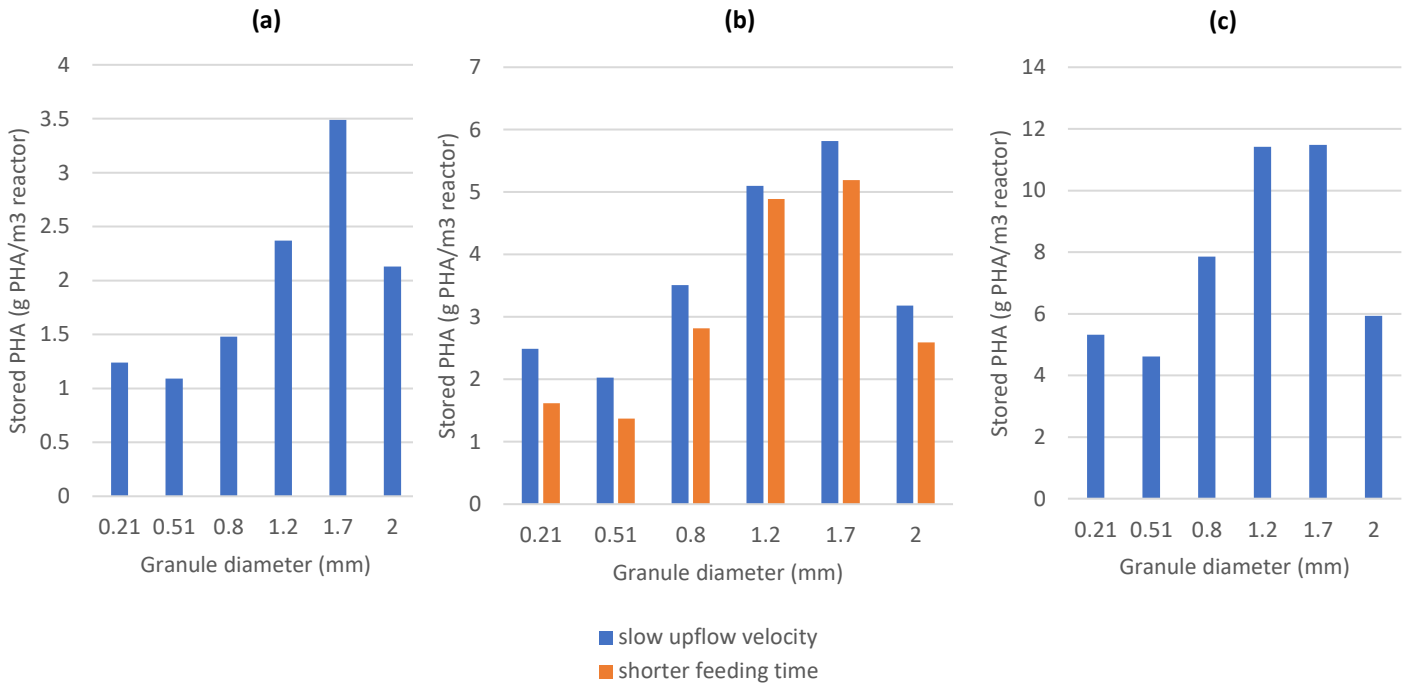


Figure 11: PHA storage per granule size with increasing exchange ratios (a) 12.5% exchange ratio, (b) 25% exchange ratio, and (c) 50% exchange ratio. For (b), the exchange ratio is showed when 25% was achieved through changing the upflow velocity versus changing the feeding time

4. Results: Pre-fermentation

To explore the practical requirements to implement pre-fermentation for AGS, an SBR fermenter was operated. Conditions influencing the stability of the fermentation process were analyzed through batch tests and by sampling from the treatment processes present prior to the fermenter intake point. The results will be discussed in this order.

Throughout the operation of the pre-fermenter, the VFA concentrations in the reactor were frequently measured within one cycle. These values were used to monitor the VFA production rates as shown in Figure 12. Two phases with different applied process controls are indicated in the figure. Phase 1 is characterized by an HRT of 8 hours and the cycle times are not related to the PNU cycles. In Phase 2, the HRT was increased to 16 hours and the feeding phase of the fermenter began at the end of the PNU feeding phase.

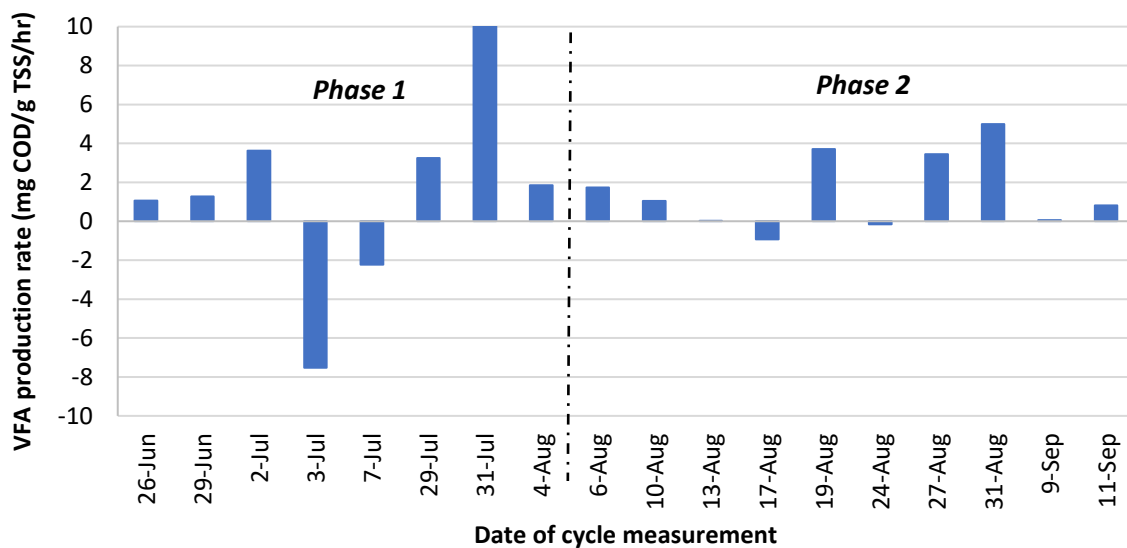


Figure 12: VFA production rate in fermenter over time . Phase 1: HRT = 8 hrs, fermenter & PNU feeding cycles not aligned. Phase 2: HRT = 16 hrs, feeding cycles aligned, the dashed line indicates the shift between phases

The average production rates, the average starting and ending VFA concentrations, and the average reactor mixed liquor suspended solid (MLSS) can be found in Table 5. On average, in one cycle, 28 mg/l VFA were produced.

Table 5: Fermenter measurements – average VFA & MLSS

VFA production (mg COD g TSS ⁻¹ h ⁻¹)	VFA – start (mg COD/l)	VFA – end (mg COD/l)	MLSS (g TSS/l)
1.5 ± 3.6	158 ± 68	186 ± 93	3.4 ± 2

Table 5 shows that there was high variability in production rates and MLSS concentrations in the reactor. This led to investigations into possible causes of the instability. Poor mixing, high selection pressure, biofilm formation, and weather conditions were all explored as possible causes of instability and found to not contribute significantly. The comparison between VFA production rates and weather conditions can be found in Appendix E. The impact of influent characteristics and the fermentation activity of biomass present in the PNU system were also investigated.

Influent VFA concentrations were measured during one feeding phase over the primary treatment for the PNU: raw influent from the pumping station, influent from mid-way in the sand trap (after

screening), and influent in the buffer tank (PNU feed). Refer to Figure 4 for a schematic of the system. The VFA concentrations over the system over time can be seen in Figure 13.

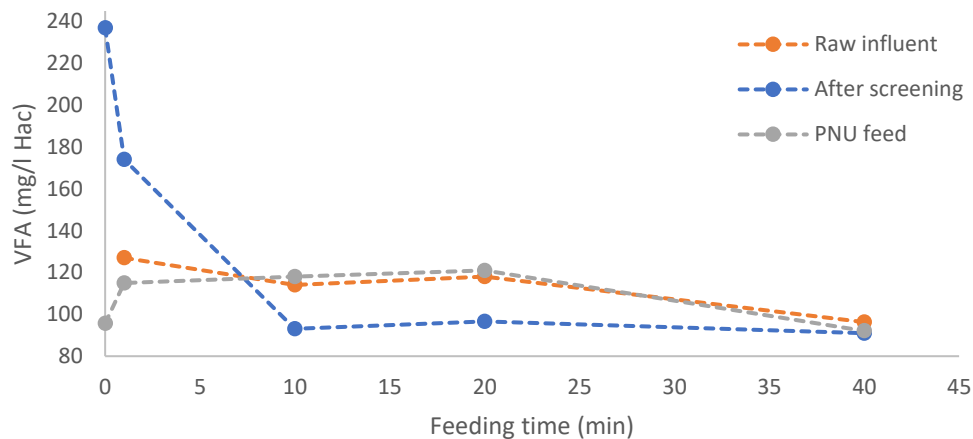


Figure 13: VFA measured in three locations in the PNU primary treatment during a feeding phase

The raw influent VFA concentrations ranged from 92 to 127 mg/l acetate, while influent after screening was from 91 to 237 mg/l, and the PNU feed was from 96 to 118 mg/l.

From these sampling events, it was determined that VFAs were being produced at a significant rate in the sand trap (after screening). This test was repeated and confirmed this conclusion, the data from this additional test can be seen in Appendix F. Based on this finding, a small sampling campaign was conducted on raw influent versus influent that had passed through the sand trap. Because of the high concentrations of VFAs produced in the sand trap, it was suspected that significant settling of degradable solids was occurring. To check if this had an influence on the influent entering the fermenter, volatile solids, settleable solids, and total COD were measured. Table 6 shows the results of these measurements. Because of the high variability in the samples, ANOVA was used to determine if there was a statistically significant difference between the influent characteristics before and after the sand trap.

Table 6: COD and VS of influent before and after sand trap. The average value with standard deviation is presented with the number of samples in the superscript

	Volatile solids (mg/l)	Total COD (mg/l)	Settleable solids (ml/L)
Raw influent	407±60 ⁶	768±59 ³	17.1±4 ⁴
Influent after sand trap	268±90 ⁹	709±42 ³	12.4±3 ⁵
Significant difference?	True	Could not be determined	Could not be determine

These results show that there was a significant drop in the volatile solids present after the sand trap compared with the raw influent. While the average total COD and settleable solids dropped as well, these differences were not significantly significant likely due to the small number of samples collected and the variability in the measured values.

To determine if there was a significant difference in the fermentation activity of the biomass present in the sand trap and that of the fermenter, several batch tests were performed.

Batch tests to ferment raw influent in eight hours were performed using different seed material: fermenter sludge, biofilm from the sand trap walls, and settled primary sludge in the sand trap. Both the fermenter sludge and settled primary sludge batch test were repeated twice with raw influent collected on different days. Corrections were made based on the VFA production observed in the blanks for influent and sludge self-fermentation. The detailed data for these tests can be found in Appendix G. The summary of results can be seen in Figure 14.

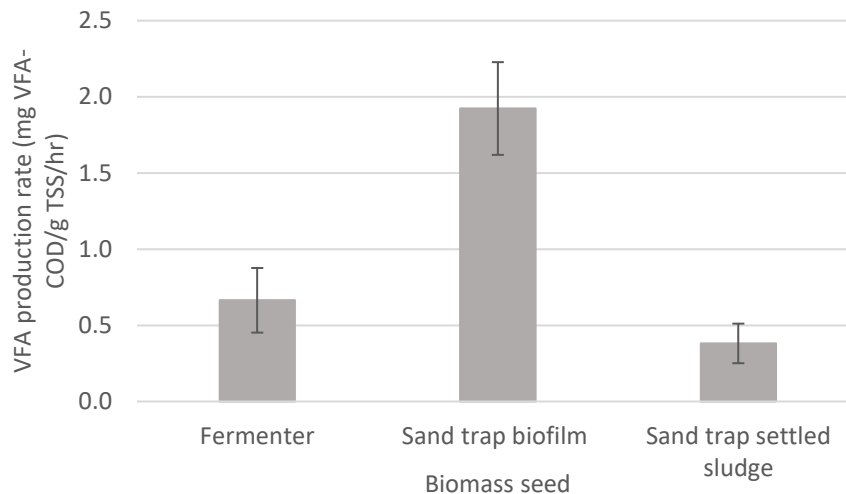


Figure 14: Eight-hour batch test: VFA production rate per biomass sample

The biofilm from the sand trap walls had a significantly higher VFA production rate than the other two seed materials. Microscopy was performed on biomass samples from the fermenter and the sand trap. These images can be found in Appendix G. Flocculent biomass can be seen in all images frequently clustered around cellulose fibers. The cellulose fibers appear to be hollow. Differences in the biomass were not observed at the measured scale.

Due to the high VFA concentrations observed in the sand trap, samples were taken over the length and depth of the sand trap to determine whether the fermentation varied with location in the sand trap. High VFA concentrations were found with high variability over the sand trap volume (see Appendix F). To clarify how this changed over the PNU cycle, measurements were done over the volume of the sand trap at the start and end of the cycle. Figure 15 shows these results.

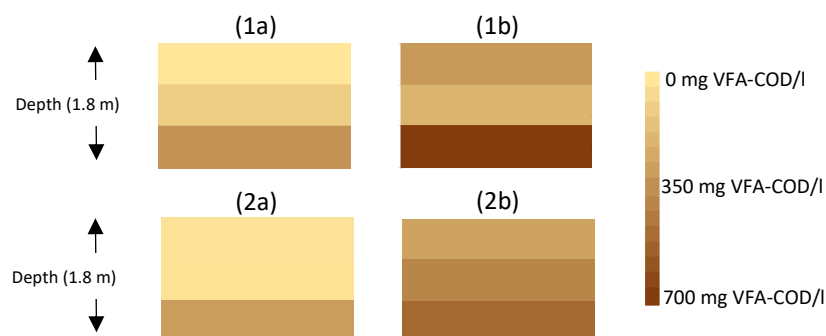


Figure 15: Variation in VFAs over the sand trap depth at two sampling points (1 = center of sand trap, 2 = end of the sand trap) at start of cycle (a) versus at the end of the cycle (b)

Significant increases in the VFA concentration were observed in all measured zones of the sand trap (from (a) to (b)) and higher VFA concentrations are present in the sludge bed. Very high concentrations are observed at the end of the cycle (250–700 mg/l) compared to the VFAs measured in the raw influent (70-150 mg/l).

To further study the VFA increase in the sand trap, samples were taken 2-3 times per week during the cycle of the PNU. During this period, the PNU cycle time was fixed, and the sand trap HRT was 8 hours. The volumetric VFA production rate averaged $21 \text{ mg VFA-COD L}^{-1} \text{ h}^{-1} \pm 15$ (raw data can be found in Appendix H).

5. Discussion

This section will discuss the results of the modeling and experimental work. Firstly, the limitations of a single granule model and the population shift from this model to the multi-granule model will be discussed. The differences between the populations in granules of different sizes will be highlighted and used to explain the differences in nutrient conversion rates when influent acetate concentrations are increased. Phosphorus uptake capacity will be discussed for the different acetate concentrations and the eventual need for SRT control in all cases. Finally, limitations of the model will be addressed. From the experimental work, the implications of the fermentation in the sand trap will be discussed along with the connection to the unstable fermenter performance. Possible other factors influencing the fermenter stability and the limitations of studying the sand trap are discussed. Additionally, the implications of the differences in fermentative activity for biomass from the PNU primary treatment system will be addressed.

5.1 Limitations of the single granule diameter model

The single granule diameter model which was used for initialization required many assumptions to describe the conversions of nutrients. This model required high concentrations of acetate to perform removal because of limitations of the mixed reactor bulk liquid. Because simultaneous nitrification denitrification was not 100%, nitrate remaining in the effluent was then present during feeding. The simulated anoxic feeding conditions led to pre-denitrification. Under plug flow feeding conditions, this would not occur as nitrate would leave the system in the decanted effluent. Additionally, without inclusion of a plug flow model, the influent was equivalently diluted and the concentration gradients (and therefore also the diffusion rate) between the bulk liquid and granules was lower than would be present with true plug flow feeding. The concentrations cannot be seen per layer, therefore, the effluent concentrations were assumed to be the concentrations present at the end of each cycle. Without modeling settling over the reactor depth, it was also not possible to perform selective spilling. These are all problems commonly encountered in modeling efforts for AGS.

While a semi-steady state was reached for the single granule model, this took upwards of 50 days to achieve (without considering wait periods or settling time as in practice). De Kreuk et al. (2007) and Baeten et al., (2018) both found steady state effluent quality was reached after 200 simulated days. Winkler et al., (2015) found steady state effluent quality and granule biomass populations after 500-800 simulated days. These periods are all significantly longer than the typically applied SRT of 30 days and in most cases longer than the SRT of 143 days found for large granules (Ali et al., 2019). This indicates that a true steady state in granules will likely never be reached in practice.

5.2 Different population shifts in different granule sizes

It was known that the semi-steady state profiles for granules of 2.2 mm diameter would not be representative of all granule sizes. This is especially true for small granules due to the low substrate availability at the top of the settled sludge bed during feeding and penetration of substrates and oxygen across the entire depth. It was expected that despite these limitations, the adapted initialization would lead to faster development to semi-steady state conditions in the multi-granule model. This proved to be an accurate assumption. In the multi-granule model, the runs undergo three stages (initialization, stable removal of nutrients, and loss of nutrient removal capacity).

The first phase, initialization, occurred as the granule species populations adapted to the new influent concentrations and the change in radius. During initialization, the species distribution in each of the granules changed due to the new granule radius and implementation of plug flow feeding into a settled sludge bed in the multi granule model. Figure 7, phase i, shows the reduction in the ammonium effluent concentrations over time due to this change in population. From Figure 8, autotrophs grew

primarily into smaller granules. Due to the low PHA storage by smaller granules located primarily at the top of the settled sludge bed (see Figure 9), there were fewer PAOs present. Due to the reduced competitive advantage for PAOs and high availability of ammonium and oxygen, nitrifying populations were larger in smaller granules. Experimental results indicated that smaller granules do indeed contribute significantly to nitrification rates in mixed AGS (Vierwind, A., 2018). The reverse explains why nitrifiers were not present in high concentrations in larger granules in addition to fact that PAOs have a higher oxygen affinity than AOB/NOB.

Heterotrophs also grew into smaller granules due to reduced competition with PAOs. While PAOs and OHOs compete aerobically for acetate uptake (Haaksman et al., 2020), OHOs can exclusively take up rbCOD at the start of aeration. In all model runs, acetate and rbCOD were present (although in small concentrations) at the start of aeration (Figure 7). This was because of the surface limitation of the larger granules at the bottom of the reactor. Acetate and rbCOD added in the last time steps of the feeding phase had limited diffusion into the large granules which already contained PHA stores and had been denitrified across the granule volume. Despite the small concentrations, the fast-growing nature of heterotrophs allowed them to establish a strong presence in the small granules.

The increase in nitrifiers in small granules while large granules contained more PAOs, demonstrates the unique role that all granule sizes play in AGS. It is necessary to have small granules in addition to large in order to optimally remove nitrogen and phosphorus. Because of this, selection pressures must not be too strict, otherwise ammonium removal capacity will be reduced or longer cycle times will be necessary. The presence of different species in granules of different sizes was identified by Ali et al. (2019), where species differed increasingly from those found in wastewater influent as granule size increased. Additionally, the mid-large size granules could be seen to have a large inert core, especially as the granule size increases. This effect has been observed in literature (McSwain et al., 2005) (Xavier et al., 2007). This is due to diffusion limitations of soluble substrates and oxygen.

Despite the large changes in species distribution for different granules sizes, the initialization phase was very short compared to models described in literature. Semi steady state conditions will never be reached in this model due to the loss of phosphorus uptake capacity (because no SRT control is applied). Once the complete removal of ammonium was achieved, stable removal of ammonium and phosphate occurred (phase ii in Figure 7). The fast stabilization of this model makes running many simulations easier.

5.3 Lack of total nitrogen removal

The concentrations of nitrate could be seen to increase during the initialization phase due to the increased nitrification performed by autotrophs. Note that the models were run as if there was an ammonium regulation but no total nitrogen regulation. Simultaneous nitrification denitrification was low in these runs. This was in part due to shallow penetration of acetate into the granule (PHA was present no deeper than 0.1 mm into the granule in the run with 100 mg/l acetate – Appendix C), and therefore, low presence of carbon donors in the anoxic zone (de Kreuk et al., 2010). The high k_{la} additionally reduced the anoxic zone in the granules. These effects were compounded by the differences in species distribution for granules of different sizes (see Figure 8). Because more autotrophs were present in small granules, nitrate must first diffuse out of the small granules and into the anoxic zone of the larger granules before denitrification could occur during the aeration phase. Because of the low SND, calibration of the model and a post anoxic phase would be necessary to denitrify.

An anoxic phase to denitrify was not modeled because the goal of the model was to determine the influence of increasing acetate concentrations in influent. At the end of the aeration cycles, no PHA

was left in the granules (see Figure 8). This is contrary to what has been observed experimentally (van den Berg, 2007). However, because of the high oxygen concentrations and k_{la} (2 mg/l DO setpoint, 10 hr^{-1} k_{la}), all PHA was used for either denitrification, poly-phosphate storage, or PAO growth. Because no acetate and rbCOD was left at the end of aeration (see Figure 6), there were no carbon donors left to denitrify. Flocculent conversion of particulate COD was not included in the model to avoid interference with the goal of the model. Because conversion of particulate COD was not included and because the residual acetate and rbCOD was consumed quickly once aeration and mixing begins, there were no carbon donors remaining to denitrify in a post-anoxic phase. However, the effect of this could be analyzed in the future with the model by adapting the flocculent population distribution during feeding and including particulate COD in the influent. This would allow for aerobic hydrolysis of particulate COD and subsequent anoxic post-denitrification.

5.4 Nutrient conversion rates

The average nutrient removal rates, during the stable removal period for each of the acetate runs, can be seen in Table 4. Ammonium removal rates increased due to increased presence of autotrophs in the small granules (see Appendix C). This could be because less rbCOD is present in the influent as acetate increased (to simulate the pre-fermentation of rbCOD to acetate) and therefore less heterotrophs were present in the small granules compared to when rbCOD concentrations were higher. This reduced the competition with autotrophs. These rates were calculated from the changes observed in the reactor bulk concentrations. Therefore, the calculated rates included the removal of ammonium and phosphate used for growth of biomass. In the future, the model can be adapted to output specific rates such as nitrification.

Simultaneous nitrification denitrification rates increased with increasing acetate due to deeper penetration of PHA in granules (see Appendix C). Phosphate release increased (see Table 1) due to increased storage of PHA with higher acetate concentrations. The increases in ammonium removal and simultaneous denitrification rates are significant because smaller reactor volumes are needed to treat the same volumes of wastewater. Cost estimations would need to be performed to consider the benefits of increasing acetate in influent against the costs of implementing fermentation.

In the multi-granule model, the cycles were shorter than would be seen in practice. This is in part due to a high k_{la} which led to fast phosphate uptake and nitrification rates to be achieved very quickly (see Figure 6). In full scale plants, more time would be required to reach the DO setpoint and the removal rates would lag behind those shown in these model results. This can be improved to model specific conditions in the future. When stable removal was achieved, phosphorus removal was completed first and the length of the aeration phase depended on the nitrification rate. The number of modeled days before stable removal occurred was therefore smaller than would occur in full scale.

5.5 Consumption of acetate by different species & the unique role of different granule sizes

The fate and role of acetate varied when the concentrations were increased. According to the stoichiometry of PHA storage in PAOs, PAOs release 0.4 mg of phosphate for every mg of acetate stored as PHA. The models for 50, 100, and 150 mg/l of acetate showed a ratio of 0.49, 0.28, and 0.26 mg P release/mg acetate respectively. The high ratio for the run with 50 mg/l acetate demonstrates that acetate was formed from rbCOD anaerobically and was then taken up by PAOs. With higher acetate concentrations, the P release per mg acetate was reduced. Considering the low rbCOD concentrations in the runs with 100 and 150 mg/l acetate, conversion of rbCOD to acetate was very low and around 28% and 35% of the acetate was consumed by other organisms in the respective runs.

In addition to influencing P release, the PHA storage across different granules varied which, in turn, influenced phosphorus removal. Increasing acetate concentrations led to increasing PHA storage for all size fractions (Figure 9). As can be seen in Figure 9, it is clear that despite the surface limitations of larger granules, granules of 1.2 mm, then 1.7 mm and 0.8 mm, stored the most PHA in the reactor. The largest granules, which came into contact with the most acetate due to their position in the settled sludge bed, were limited by their low efficiency (due to surface limitations) and had significantly less PHA storage than most of the other granules. These factors contributed to the removal of phosphate in the system as can be seen in Figure 10. Granules of 1.7 mm performed the most phosphate removal, followed by 2 mm and 1.2 mm granules. This shows that there is an optimal granule size for phosphate removal. Even though the 2 mm granules had the most contact with acetate in the influent, they were limited in their PHA uptake and phosphate removal. By implementing more stringent SRT control and removing the largest granules, the phosphate removal can be optimized. While this model showed that 1.7 mm granules were the most effective, the actual diameter will differ in practice. This model showed the principle that stricter SRT control can improve the phosphate removal capacity. A balance must be found between optimization of granule size for phosphorus removal and maintaining a well settling granule bed.

5.6 Loss of phosphate uptake capacity without SRT control

The role of poly-phosphate uptake over granule sizes also related to the loss of phosphate uptake capacity which was observed in all runs. In the model, the granules were not controlled on SRT. The effect of redistributing the species controlled the total biomass concentration in the reactor but did not implement necessary actions that SRT control performs in real reactors. Namely, without SRT control, granules accumulated poly-phosphate until they approached their maximum poly-phosphate storage capacity (from ASM2d, 0.34 mg PP/mg PAO) (de Kreuk et al. 2007). Figure 10 shows reducing rates of phosphorus removal as poly-phosphate saturation was approached for all granule sizes. Therefore, over time, uptake was reduced, and effluent phosphate concentrations increased.

In practice, the loss of phosphate uptake capacity is slower. The model shows that this occurred in less time than typically applied SRTs. The slower process in practice could be related to the effect of shear on granules (which is not included in the model). It is expected that outer layers of the granule are sheared off and this makes up part of the “flocculent” biomass that is spilled. This process would allow for growth of PAOs in granules layers which are not saturated with poly-phosphate. In practice there are additional factors which influence phosphate uptake capacity such as loss of larger granules in the spill and rain weather events where changes in loading influence the effluent quality short term.

5.7 Stability of phosphate uptake capacity with higher acetate concentrations

The higher the acetate concentrations, the longer the phosphate uptake capacity was stable. This is notable because despite that all runs used the same phosphate concentrations in the influent and the granules had the same maximum poly-phosphate storage, higher acetate increased the stability of phosphorus removal. When acetate concentrations were low, the PHA storage for all granules was lower. Because this increases with more acetate, more poly-phosphate could be removed. Additionally, the stratification of the granule sizes over the bed influenced phosphorus removal. The larger granules took up the most acetate and then stored the most poly-phosphate initially (see Figure 10). This means that larger granules also approached the maximum poly-phosphate capacity faster. After a number of runs (as seen in Figure 7), larger granules had reached capacity, but the smaller granules had not. However, large granules continued to take up acetate and store PHA during feeding, even when they had reduced poly-phosphate capacity. This means that when the acetate concentrations were low, and less acetate reached the smaller granules at the top of the sludge bed, the granules which had remaining poly-phosphate storage capacity did not have the necessary PHA stores to do so. When acetate concentrations were higher, these granules could continue to perform

uptake until they also reached their capacity. The loss in poly-phosphate storage capacity could be seen as a reduction in phosphate uptake rate during the cycle.

5.8 Influence of exchange ratios on AGS performance

The influence of exchange ratios is a unique topic which could be explored with the model. The change in substrate penetration through the sludge bed during feeding could be seen to have an effect on the PHA storage distribution over granules of different sizes (Figure 11). Firstly, a comparison was made by changing the exchange ratio through applying different upflow velocities. This had an influence on the expansion of the sludge bed during feeding and the amount of time that each layer in the sludge bed had contact with substrate. Larger batch sizes led to deeper penetration of the substrate front into the sludge bed. This is why the larger granules of 1.7 mm diameter took up a larger amount of PHA compared to other granule sizes and this effect was amplified by applying lower exchange ratios.

These findings can be used to improve granulation processes. For example, when granulation begins, it is optimal to ensure growth of PAOs in all granule sizes, and therefore a larger exchange ratio is preferable. Once granules are growing, the exchange ratio can be adapted to encourage growth of the overall bed or target the larger granules by enriching them with PHA through smaller exchange ratios.

The effect of exchange ratios is difficult to elucidate with one set of simulations or experimentally. A specific exchange ratio can be achieved by changing the upflow velocity or the anaerobic feeding time and both will have a unique effect. An additional run for the 25% exchange ratio showed the difference that occurred when anaerobic feeding time was altered in place of upflow velocity. In Figure 11b, shorter feeding time limited how much VFA could be taken up; a larger penetration of substrate into the sludge bed was observed (68% compared to 59%, see Appendix J for examples of this effect) because of this. Shorter contact time also reduced how much rbCOD could be fermented to acetate and stored as PHA. Therefore, only 74% of the loaded acetate was stored as PHA when shorter feeding times were applied compared to 89%. Additionally, applying a shorter feeding time resulted in a larger difference between the PHA stored in granules of 0.51 mm (the ones which received the least) and the PHA in granules of 1.7 mm (the ones which received the most). However, in the cases with lower exchange ratios, it was expected that the smaller granules would receive significantly less acetate than larger granules. This effect was not as strong as anticipated.

Changing upflow velocity or anaerobic feeding time without changing the influent concentrations will lead to a change in loading. This makes it particularly difficult to understand which factor led to a result experimentally. This model setup gives the opportunity to examine all these factors to optimize operation depending on the specific goal.

5.9 Model limitations

While the model can demonstrate principles that have been hypothesized, there are limitations, including:

1. Glycogen accumulating organisms (GAOs) are not included

ASM2d kinetics do not include GAOs which can compete with PAOs for substrate in practice (Oehman et al., 2010). Because GAOs do not contribute to phosphate removal, this leads to a higher required carbon loading to achieve stable phosphate removal. Without competition with GAOs, the PAOs in this model receive more acetate and more phosphate uptake capacity is possible in the reactor.

2. All VFAs are modeled as acetate

Different PAO and GAO species can store acetate versus propionate as PHA. ASM2d kinetics include a very simplified conversion which neglects the variability in metabolic pathways which are present. However, the use of these complex metabolic pathways leads to difficulty in calibration of a high number of model parameters (van Loosdrecht et al., 2008). Because the COD division selected for the model does not include division of VFAs into acetate, propionate, and higher weight VFAs, the concentrations of modeled acetate are higher than would be present in practice. However, these divisions do not influence the principles which are demonstrated in the model. For further investigation into pre-fermentation, these factors should be considered.

3. Glycogen is not included

Glycolysis drives the storage of acetate as PHA and release of poly-phosphate stores. The model does not include glycogen however this is an important factor, especially when PHA stores are low. Because the model reaches depletion of PHA stores, this would influence the results.

4. Chemical phosphorus reactions are not included

Phosphorus removal does not only occur biologically, there are also precipitation reactions that occur (de Kreuk et al., 2005). Precipitation is pH sensitive and because increases in VFA can reduce the pH, this warrants future consideration.

5.10 Implications of fermentation observed in the sand trap

The model demonstrated that increasing acetate concentrations improved stability of phosphate uptake capacity and increased simultaneous nitrification denitrification rates. This demonstrated the improvements which are possible through pre-fermentation. The experimental results showed that the sand trap at the PNU in Utrecht unintentionally performed significant pre-fermentation (rates of $21 \text{ mg COD L}^{-1} \text{ hr}^{-1} \pm 15$). The horizontal velocity of the flow through the sand trap was between 0.02-0.03 m/s, significantly lower than the standard 0.3 m/s which is applied for grit removal (Metcalf et al., 1979). As the standard design for grit removal aims to remove sand particles and leave organic matter in suspension, this low flow rate led to settlement of degradable organic matter. In addition, despite the large accumulation of particles in the sand trap, cleaning was performed infrequently (2 cleanings were performed during the year that this thesis spanned). Organic particles could, therefore, remain in the sand trap for months or until they were hydrolyzed. Flow of influent through the sand trap only occurred during the PNU feeding phase. During these experiments, the time between feeding phases was around 8 hours. The combination between the slow flow rate and the batch operation of the sand trap allowed for hydrolysis and fermentation to occur. This effect could be optimized in practice to achieve fermentation. The rates observed in the sand trap are high enough to provide sufficient additional phosphorus removal capacity at domestic WWTPs which currently struggle to meet regulations.

5.11 Limitations of studying sand trap fermentation

While the sand trap operated simultaneously as a pre-fermenter, it was difficult to obtain information with certainty about the operation. Due to the variability in sludge height observed over the length of the sand trap and over time, an exact SRT and liquid volume could not be determined. Most of the measured rates were based on measurements from a single sampling point over a cycle. The volume was unmixed (except in the case of gas release, which was observed) and therefore these point measurements only gave an indication of the fermentation. Additionally, variables such as weather and operational changes (such as shorter cycles, skipped feeding phases, etc.) influenced the conditions in the sand trap. Because these measured rates were indication values, these outside

factors were not compared against the data. These factors should be considered for future research. It is recommended to study fermentation further at a smaller scale to control these factors more easily.

5.12 Unstable performance in fermenter

The factors which led to fermentation in the sand trap also likely led to instable fermentation in the fermenter. As can be seen from Figure 12, the fermenter VFA production rates varied considerably. Rates typically ranged from -2 to 5 mg COD g TSS⁻¹ h⁻¹. However, on average, 28 mg/l VFA were produced in a cycle. Considering that 20 mg/l VFA can remove an additional 1 mg/l P, this production was enough to remove at least 1.4 mg/l P. This would make it easier for some WWTPs to meet the effluent requirements without iron dosing. Literature indicates that rates up to 19 mg VFA g TSS⁻¹ hr⁻¹ can be achieved on influent (Gonzalez Barelo et al., 2006, Ligeró et al. 2001a, Alvarez et al. 2003, Alvarez et al. 2008, Cuevas and Tejero, 2003, Donoso-Bravo et al., 2009). The cause of the negative rates could not be identified but could be due to presence of methanogens washing in from the sewer or volatilization of VFAs into the headspace. A low mixing rate was applied to avoid this volatilization but gas measurements from an airtight headspace would be necessary to elucidate the cause of VFA loss.

For Phase 2, when the HRT was extended to 16 hours, it was no longer possible to manually sample at the start and end of the cycle. The calculated rates are therefore based on the rates over the 8 hours which were measurable during the open hours at the WWTP. An increase in MLSS was expected if longer HRTs improved the fermentation in the reactor, and this was not observed. In future experiments, a system for automated sampling and keeping sample volumes cool would be recommended.

5.13 Connection between high fermentation in sand trap and low fermentation in fermenter

The fermenter pumped influent from the buffer tank (see schematic in Figure 4). During phase 1, the feeding phase for the fermenter was not linked to the PNU cycles. This meant that the fermenter fed when the influent in the buffer tank was likely already fermented to a degree and solids had settled (and therefore were not pumped into the fermenter). Once the fermenting behavior of the sand trap was identified, the cycles were linked (Phase 2) so that the fermenter only fed if the PNU had influent flowing through the buffer tank. From Figure 13, it can be seen that at the end of the feeding phase, the VFA concentrations in the buffer tank were similar to those in the raw influent. This demonstrated that VFAs were flushed out of the sand trap at the start of feeding but that the influent at the end of the feeding phase was not pre-fermented.

Despite the changes implemented for Phase 2, the fermenter performance did not stabilize. Upon further investigation, the influent that the fermenter received had significantly fewer volatile solids (see data in Table 4). The difference between raw influent and influent after passing through the sand trap was significant despite the small number of samples (n=6 for raw influent & n=9 for influent after the sand trap). Even fewer samples were compared for COD and settleable solids. Therefore, more samples would be required to determine with certainty that the fermenter received less COD and settleable solids. However, considering the loss in volatile solids, this is likely. This is linked to the operation of the sand trap. Because the flow rate is too low, the solids were settled out in advance. Therefore, the fermenter had less available substrate to degrade.

5.14 Possible other factors for unstable fermenter performance

As mentioned, additional factors were considered when investigating the instability of the fermenter. Checks were performed to determine if the mixing was insufficient which could lead to limited contact

time between the sludge and the influent or could cause inaccurate measurements of MLSS and VFA. Settling tests were performed on the sludge to check if the selection pressure was appropriate to ensure that excessive sludge discharge was not occurring each cycle. Because of the possibility that methanogens were consuming the VFAs, the SRT in the system was verified. A check was performed for solids that settled too quickly to be measured in the MLSS and for the presence of a biofilm which could have an infinite SRT. Finally, a connection between the variations in performance and weather conditions were checked (Appendix E). None of these possibilities were found to have an influence.

5.15 Different fermentative activity observed in biomass across the PNU

Comparisons were made between the biomass in the fermenter and that present in the sand trap settled solids and in a biofilm layer on the sand trap walls. Microscopy showed little visible difference between the biomass at the investigated scale (see Appendix G). This is in line with expectations as similar feed composition is available and similar microbial communities are present in the sewer and in wastewater treatment systems (Huisman and Gujer, 2002). However, when each biomass was added to batch tests to ferment raw influent, the biofilm from the sand trap walls had significantly higher fermentation capacity (Figure 14). This could be because the biofilm has a longer retention time than the settled solids. However, it is unclear what the retention time of the solids in the sand trap is. The settled solids and the fermenter sludge had similar activities. This is to be expected because the fermenter was seeded with these settled solids at the start of Phase 2. The sand trap has a surface area to volume ratio of $1.1 \text{ m}^2/\text{m}^3$. Additionally, there is a thick layer of accumulated fats on the sand trap walls. This could give the opportunity for a relatively thick biofilm layer to grow. Systems with high surface area like moving bed biofilm reactor (MBBR) and integrated fixed-film activated sludge (IFAS) have significantly higher surface area to volume ratios, ranging from $50\text{-}335 \text{ m}^2/\text{m}^3$ (Sen et al., 2006). Addition of carrier materials to the fermenter could allow for an increased surface area with sufficient retention time for biomass. However, this could lead to problems even at the pilot scale including growth of methanogens with difficult SRT control.

6. Conclusions

The model demonstrated principles observed in practice at AGS plants which have not been previously successfully modeled. The confirmation of these principles shows high potential for the application of this model for further research.

The novel principles described by the model (ordered according to the relevant research question) include:

1. Demonstration that increasing acetate concentrations leads to longer stability of phosphorus uptake capacity in the system and demonstration of the inevitable requirement for SRT control due to saturation of poly-phosphate stores. This has been observed as a problem in practice at low loaded plants.
2. Demonstrations that increasing acetate concentrations leads to increasing phosphate release and simultaneous nitrification denitrification. Therefore, reactor size can be reduced if acetate concentrations are increased.
3. Demonstrate the presence of (and necessity of) different species dominance in granules of different sizes due to plug flow feeding in a settled granule bed: PAOs are dominant in larger granules and nitrifiers are dominant in smaller granules. This means that nitrate is formed in small granules and must be transported through the bulk liquid to larger granules to be denitrified. Demonstration of reduced efficiency of granules with increasing diameter and the existence of a maximum granule size for optimal phosphate removal (1.7 mm).
4. Demonstration that there is a granule size which receives the most acetate and subsequently removes the most phosphate, and this effect is more prominent when the exchange ratio is small. Maintaining long feeding times is necessary to optimize storage of acetate as PHA.

These novel results demonstrate the benefit of combining models to describe settling of AGS, plug flow feeding in a settled sludge bed, reaction in the bulk and in granules, and diffusion across granules and into bulk liquid. The integrations of these models with granules of different sizes revealed the importance of acetate concentrations in low loaded domestic wastewaters and the potential improvements to process stability which pre-fermentation could provide.

The experimental pre-fermentation results demonstrated that fermentation can occur in high rates in batch systems receiving enough biodegradable substrates. In the sand trap, fermentation was achieved with a rate of $21 \text{ mg VFA-COD L}^{-1} \text{ h}^{-1} \pm 15$ with a horizontal velocity of 0.02 m/s and an HRT of 8 hours. Unstable fermentation occurred in an SBR fermenter due to settling of biodegradable solids in the prior treatment system: the sand trap. The fermenter produced 28 mg VFA/l on average. Both systems could produce enough VFAs on average to significantly improve phosphorus removal. More research is needed to determine the optimal operational conditions to ferment influent and to demonstrate the effect on aerobic granular sludge in practice.

7. Recommendations

This research can be expanded and connected to other topics being researched presently. Below, a list of recommendations related to extending the model and simulations to consider as well as further research into pre-fermentation are suggested.

Modeling

1. Implement flocculent conversion of particulates (must adapt the distribution of flocs during feeding to implement properly).
2. Adjust the model parameters to avoid depletion of PHA. Additionally, glycogen should be included in the model.
3. Growth and wasting of sludge and the effect of shear can be implemented.
4. Many different simulations can be run including:
 - a. Anaerobic feeding time
 - b. Fermentation during feeding
 - c. K_{la} & oxygen setpoint
 - d. Selection pressure
 - e. Startup strategy
 - f. SRT optimization

Pre-fermentation

1. Relocate fermenter to receive fresh influent and can then optimize the operation by exploring the effect of HRT, SRT, temperature, and settling rates.
2. The effect of pre-fermentation can be coupled with AGS experimentally.
3. Biochemical acidogenic potential (BAP) tests (Ruel et al., 2001) should be performed on any potential influent being considered for pre-fermentation (specifically from the location in the treatment train where fermentation would be implemented).

References

- Abu-Ghararah, Z., & Randall, C. (1991). The effect of organic compounds on biological phosphorus removal. *Water Science and Technology*, 23(4-6), 585–594.
- Association, A. P. H., Association, A. W. W., Federation, W. P. C., & Federation, W. E. (1915). *Standard methods for the examination of water and wastewater* (Vol. 2). American Public Health Association.
- van den Berg, L. (2017). *Characterization and Modelling of Full-Scale Aerobic Granular Sludge*. Delft University of Technology MSc. Thesis.
- Beun, J., Heijnen, J., & Van Loosdrecht, M. (2001). N-removal in a granular sludge sequencing batch airlift reactor. *Biotechnology and Bioengineering*, 75(1), 82–92.
- Beun, J., Hendriks, A., Van Loosdrecht, M., Morgenroth, E., Wilderer, P., & Heijnen, J. (1999). Aerobic granulation in a sequencing batch reactor. *Water Research*, 33(10), 2283–2290.
- Bouzas, A., Ribes, J., Ferrer, J., & Seco, A. (2007). Fermentation and elutriation of primary sludge: Effect of srt on process performance. *Water Research*, 41(4), 747–756.
- de Bruin, L., De Kreuk, M., Van Der Roest, H., Uijterlinde, C., & Van Loosdrecht, M. (2004). Aerobic granular sludge technology: An alternative to activated sludge? *Water Science and Technology*, 49(11-12), 1–7.
- Carlson, G., & Silverstein, J. (1998). Effect of molecular size and charge on biofilm sorption of organic matter. *Water Research*, 32(5), 1580–1592.
- Crank, J., & Nicolson, P. (1947). A practical method for numerical evaluation of solutions of partial differential equations of the heat-conduction type. In *Mathematical Proceedings of the Cambridge Philosophical Society* (Vol. 43, No. 1, pp. 50-67). Cambridge University Press.
- Cussler, E. L., (2009). *Diffusion: mass transfer in fluid systems*. Cambridge university press.
- Danesh, S., & Oleszkiewicz, J. A. (1997). Use of a new anaerobic-aerobic sequencing batch reactor system to enhance biological phosphorus removal. *Water Science and Technology*, 35(1), 137–144.
- Dangcong, P., Bernet, N., Delgenes, J.-P., & Moletta, R. (1999). Aerobic granular sludge—a case report. *Water Research*, 33(3), 890–893.
- Degaleesan, S., & Duduković, M. P. (1998). Liquid backmixing in bubble columns and the axial dispersion coefficient. *AIChE journal*, 44(11), 2369-2378.
- van Dijk, E. J., Pronk, M., & van Loosdrecht, M. C. (2018). Controlling effluent suspended solids in the aerobic granular sludge process. *Water research*, 147, 50-59.
- van Dijk, E., Pronk, M., & van Loosdrecht, M. (2020). A settling model for full-scale aerobic granular sludge. *Water Research*, 116–135.
- van Dijk, E. J. H., van Schagen, K. M., & Oosterhoff, A. T. (2020). *U.S. Patent Application No. 16/693,113*.
- Dold, P., Alexander, B., Burger, G., Fairlamb, M., Conidi, D., Bye, C., & Du, W. (2018). Modeling full-scale granular sludge sequencing tank performance. *Proceedings of the Water Environment Federation*, 2018(10), 3813-3826.

- Fan, L. T., Yang, Y. C., & Wen, C. Y. (1960). Mass transfer in semifluidized beds for solid-liquid system. *AIChE Journal*, 6(3), 482-487.
- Haaksman, V. A., Mirghorayshi, M., van Loosdrecht, M. C. M., & Pronk, M. (2020). Impact of aerobic availability of readily biodegradable COD on morphological stability of aerobic granular sludge. *Water Research*, 187, 116402.
- Hauduc, H., Rieger, L., Takács, I., Héduit, A., Vanrolleghem, P., & Gillot, S. (2010). A systematic approach for model verification: Application on seven published activated sludge models. *Water Science and Technology*, 61(4), 825–839.
- Heijnen, J., van Loosdrecht, M. (1998). Method for Acquiring Grain-Shaped Growth of a Microorganism in a Reactor. *WO 9837027 (A1)*
- Henze, M., Gujer, W., Mino, T., & van Loosdrecht, M. C. (2000). *Activated sludge models asm1, asm2, asm2d and asm3*. IWA publishing.
- Henze, M., van Loosdrecht, M. C., Ekama, G. A., & Brdjanovic, D. (2008). *Biological wastewater treatment*. IWA publishing.
- Huisman, J. L., & Gujer, W. (2002). Modelling wastewater transformation in sewers based on ASM3. *Water science and technology*, 45(6), 51-60.
- de Kreuk, M. K., Heijnen, J. J., & Van Loosdrecht, M. C. M. (2005). Simultaneous COD, nitrogen, and phosphate removal by aerobic granular sludge. *Biotechnology and bioengineering*, 90(6), 761-769.
- de Kreuk, M., Kishida, N., Tsuneda, S., & Van Loosdrecht, M. (2010). Behavior of polymeric substrates in an aerobic granular sludge system. *Water Research*, 44(20), 5929–5938.
- de Kreuk, M., Kishida, N., & Van Loosdrecht, M. (2007). Aerobic granular sludge—state of the art. *Water Science and Technology*, 55(8-9), 75–81.
- de Kreuk, M. K., & van Loosdrecht, M. C. (2006). Formation of aerobic granules with domestic sewage. *Journal of Environmental Engineering*, 132(6), 694–697.
- de Kreuk, M., Picioreanu, C., Hosseini, M., Xavier, J., & Van Loosdrecht, M. (2007). Kinetic model of a granular sludge sbr: Influences on nutrient removal. *Biotechnology and Bioengineering*, 97(4), 801–815.
- Layer, M., Adler, A., Reynaert, E., Hernandez, A., Pagni, M., Morgenroth, E., Holliger, C., & Derlon, N. (2019). Organic substrate diffusibility governs microbial community composition, nutrient removal performance and kinetics of granulation of aerobic granular sludge. *Water Research X*, 4, 100033.
- Layer, M., Villodres, M. G., Hernandez, A., Reynaert, E., Morgenroth, E., & Derlon, N. (2020). Limited simultaneous nitrification-denitrification (snd) in aerobic granular sludge systems treating municipal wastewater: Mechanisms and practical implications. *Water Research X*, 100048.
- van Loosdrecht, M. C. M., & Heijnen, J. J. (2002). Modelling of activated sludge processes with structured biomass. *Water Science and Technology*, 45(6), 13-23.
- Lu, H., Keller, J., & Yuan, Z. (2007). Endogenous metabolism of *Candidatus Accumulibacter phosphatis* under various starvation conditions. *Water Research*, 41(20), 4646–4656.
- Metcalf, L., Eddy, H. P., & Tchobanoglous, G. (1979). *Wastewater engineering: Treatment, disposal, and reuse* (Vol. 4). McGraw-Hill New York.

- Miron, Y., Zeeman, G., Van Lier, J. B., & Lettinga, G. (2000). The role of sludge retention time in the hydrolysis and acidification of lipids, carbohydrates and proteins during digestion of primary sludge in cstr systems. *Water Research*, 34(5), 1705–1713.
- Morgenroth, E., Kommedal, R., & Harremoës, P. (2002). Processes and modeling of hydrolysis of particulate organic matter in aerobic wastewater treatment—a review. *Water Science and Technology*, 45(6), 25–40.
- Morgenroth, E., Sherden, T., Van Loosdrecht, M., Heijnen, J., & Wilderer, P. (1997). Aerobic granular sludge in a sequencing batch reactor. *Water Research*, 31(12), 3191–3194.
- Münch, E. v, & Koch, F. (1999). A survey of prefermenter design, operation and performance in australia and canada. *Water Science and Technology*, 39(6), 105–112.
- Nicholls, H., Pitman, A., & Osborn, D. (1985). The readily biodegradable fraction of sewage: Its influence on phosphorus removal and measurement. *Water Science and Technology*, 17(11-12), 73–87.
- Oehmen, A., Carvalho, G., Lopez-Vazquez, C. M., Van Loosdrecht, M. C. M., & Reis, M. A. M. (2010). Incorporating microbial ecology into the metabolic modelling of polyphosphate accumulating organisms and glycogen accumulating organisms. *Water research*, 44(17), 4992-5004.
- Pronk, M., Abbas, B., Al-Zuhairy, S. H. K., Kraan, R., Kleerebezem, R., & Van Loosdrecht, M. C. M. (2015). Effect and behaviour of different substrates in relation to the formation of aerobic granular sludge. *Applied microbiology and biotechnology*, 99(12), 5257-5268.
- Pronk, M., De Kreuk, M., De Bruin, B., Kamminga, P., Kleerebezem, R. van, & Van Loosdrecht, M. (2015). Full scale performance of the aerobic granular sludge process for sewage treatment. *Water Research*, 84, 207–217.
- Richardson, J. F., & Zaki, W. N. (1954). Sedimentation and fluidisation: Part I. *Chemical Engineering Research and Design*, 75, S82-S100.
- Ruel, S. M., Comeau, Y., Heduit, A., Deronzier, G., Ginestet, P., & Audic, J. (2002). Operating conditions for the determination of the biochemical acidogenic potential of wastewater. *Water Research*, 36(9), 2337–2341.
- Schroeten, I. (2019). *The influence of available cod on denitrification* [Master's thesis]. TU Delft.
- Sen, D., Copithorn, R. R., & Randall, C. W. (2006). Successful Evaluation of Ten IFAS and MMBR Facilities by applying the Unified Model to Quantify Biofilm Surface Area Requirements for Nitrification, Determine its Accuracy in Predicting Effluent Characteristics, and understand the Contribution of Media towards Organics Removal and Nitrification. *Proceedings of the Water Environment Federation*, 2006(13), 185-199.
- Smolders, G.J.F. (1995). *A metabolic model of the biological phosphorus removal. Stoichiometry, kinetics and dynamic behaviour*. Delft University of Technology Doctoral dissertation.
- Su, K.-Z., & Yu, H.-Q. (2006). A generalized model for aerobic granule-based sequencing batch reactor. 1. Model development. *Environmental Science & Technology*, 40(15), 4703–4708.
- Vierwind, A. (2018). *Characterisation of the influence of oxygen concentration, granule size and COD depletion on the N-removal rates of full-scale grown Aerobic Granular Sludge* [Master's thesis]. TU Delft.

Wagner, J., Weissbrodt, D. G., Manguin, V., Costa, R. H. R. da, Morgenroth, E., & Derlon, N. (2015). Effect of particulate organic substrate on aerobic granulation and operating conditions of sequencing batch reactors. *Water Research*, *85*, 158–166.

Winkler, M.-K., Le, Q. H., & Volcke, E. I. (2015). Influence of partial denitrification and mixotrophic growth of nob on microbial distribution in aerobic granular sludge. *Environmental Science & Technology*, *49*(18), 11003–11010.

Yuan, Q., Gong, H., Xi, H., & Wang, K. (2020). Aerobic granular sludge formation based on substrate availability: Effects of flow pattern and fermentation pretreatment. *Frontiers of Environmental Science & Engineering*, *14*(3), 1–10.

Yuan, Q., Sparling, R., & Oleszkiewicz, J. (2011). VFA generation from waste activated sludge: Effect of temperature and mixing. *Chemosphere*, *82*(4), 603–607.

Appendix A: Model matrices & parameters

	Oxygen (gO ₂ /m ³) S_O	Fermentables (gCOD/m ³) S_F	Acetate (gCOD/m ³) S_A	Ammonium & Ammonia (g N/m ³) S_NH4	Dinitrogen (g N/m ³) S_N2	Nitrate & Nitrite nitrogen (g N/m ³) S_NO3	Phosphorus (g P/m ³) S_PO4	Inerts (g COD/m ³) X_I	Slowly biodegradable substrates (g COD/m ³) X_S	Heterotrophs (g COD/m ³) X_H	PAO (g COD/m ³) X_PAO	Poly-phosphate (g P/m ³) X_PP	PHA (g COD/L) X_PHA	Nitrifying organisms (g COD/m ³) X_A
Aerobic hydrolysis	0	1	0	0.01	0	0	0	0	-1	0	0	0	0	0
Anoxic hydrolysis	0	1	0	0.01	0	0	0	0	-1	0	0	0	0	0
Anaerobic hydrolysis	0	1	0	0.01	0	0	0	0	-1	0	0	0	0	0
Heterotrophic growth on sf	-0.6	-1.6	0	-0.022	0	0	-0.004	0	0	1	0	0	0	0
Heterotrophic growth on sa	-0.6	0	-1.6	-0.07	0	0	-0.02	0	0	1	0	0	0	0
Heterotrophic denitrification with sf	0	-1.6	0	-0.022	0.21	-0.21	-0.004	0	0	1	0	0	0	0
Heterotrophic denitrification with sa	0	0	-1.6	-0.07	0.21	-0.21	-0.02	0	0	1	0	0	0	0
Heterotrophic fermentation of sf	0	-1	1	0.03	0	0	0.01	0	0	0	0	0	0	0
Heterotrophic lysis	0	0	0	0.031	0	0	0.01	0.1	0.9	-1	0	0	0	0
PAO storage PHA	0	0	-1	0	0	0	0.4	0	0	0	0	-0.4	1	0
PAO aerobic storage PP	-0.2	0	0	0	0	0	-1	0	0	0	0	1	-0.2	0
PAO anoxic storage PP	0	0	0	0	0.07	-0.07	-1	0	0	0	0	1	-0.2	0
PAO growth on sa aerobic	-0.6	0	0	-0.07	0	0	-0.02	0	0	0	1	0	-1.6	0
PAO growth on sa anoxic	0	0	0	-0.07	0.21	-0.21	-0.02	0	0	0	1	0	-1.6	0
PAO lysis	0	0	0	0.031	0	0	0.01	0.1	0.9	0	-1	0	0	0
PP lysis	0	0	0	0	0	0	1	0	0	0	0	-1	0	0
PHA lysis	0	0	1	0	0	0	0	0	0	0	0	0	-1	0
Autotrophic growth	-18	0	0	-4.24	0	4.17	-0.02	0	0	0	0	0	0	1
Autotroph lysis	0	0	0	0.031	0	0	0.01	0.1	0.9	0	0	0	0	-1

Rates

Aerobic hydrolysis	$K_{hyd} \cdot \lim_{O_hyd} \cdot \lim_{sur_hyd} \cdot X_H$
Anoxic hydrolysis	$K_{hyd} \cdot \eta_{NO3_hyd} \cdot \lim_{NO3_hyd} \cdot \lim_{sur_hyd} \cdot X_H$
Anaerobic hydrolysis	$K_{hyd} \cdot \eta_{fe_hyd} \cdot \lim_{sur_hyd} \cdot X_H$
Heterotrophic growth on sf	$\mu_H \cdot \lim_{O_H} \cdot \lim_{F_H} \cdot \text{cons}_F \cdot X_H$
Heterotrophic growth on sa	$\mu_H \cdot \lim_{O_H} \cdot \lim_{A_H} \cdot \text{cons}_A \cdot X_H$
Heterotrophic denitrification with sf	$\mu_H \cdot \eta_{NO3_H} \cdot \lim_{NO3_H} \cdot \lim_{F_H} \cdot \text{cons}_F \cdot X_H$
Heterotrophic denitrification with sa	$\mu_H \cdot \eta_{NO3_H} \cdot \lim_{NO3_H} \cdot \lim_{A_H} \cdot \text{cons}_A \cdot X_H$
Heterotrophic fermentation of sf	$q_{fe} \cdot \lim_{Fe_H} \cdot X_H$
Heterotrophic lysis	$b_H \cdot X_H$
PAO storage PHA	$q_{PHA} \cdot \lim_{A_PAO} \cdot \lim_{stor_PP} \cdot X_{PAO}$
PAO aerobic storage PP	$q_{PP} \cdot \lim_{O_PAO} \cdot \lim_{PS_PAO} \cdot \lim_{stor_PHA} \cdot \lim_{stor_PP_max} \cdot X_{PAO}$
PAO anoxic storage PP	$q_{PP} \cdot \eta_{NO3_PAO} \cdot \lim_{O_PAO} \cdot \lim_{PS_PAO} \cdot \lim_{NO3_PAO} \cdot \lim_{stor_PHA} \cdot \lim_{stor_PP_max} \cdot X_{PAO}$
PAO growth on sa aerobic	$\mu_{PAO} \cdot \lim_{O_PAO} \cdot \lim_{stor_PHA} \cdot X_{PAO}$
PAO growth on sa anoxic	$\mu_{PAO} \cdot \eta_{NO3_PAO} \cdot \lim_{O_PAO} \cdot \lim_{NO3_PAO} \cdot \lim_{stor_PHA} \cdot \lim_{O_PAO} \cdot X_{PAO}$
PAO lysis	$b_{PAO} \cdot X_{PAO} \cdot \lim_{O_PAO}$
PP lysis	$b_{PP} \cdot X_{PP} \cdot \lim_{O_PAO}$
PHA lysis	$b_{PHA} \cdot X_{PHA} \cdot \lim_{O_PAO}$
Autotrophic growth	$\mu_A \cdot \lim_{O_A} \cdot \lim_{NH4_A} \cdot X_A$
Autotroph lysis	$b_A \cdot X_A$

Terms to calculate rates

Abbreviations

$S_{O}/(K_{O_hyd}+S_{O})$	\lim_{O_hyd}
$K_{O_hyd}/(K_{O_hyd}+S_{O})$	\lim_{O_hyd}
$S_{O}/(K_{O_H}+S_{O})$	\lim_{O_H}
$K_{O_H}/(K_{O_H}+S_{O})$	\lim_{O_H}
$S_{O}/(K_{O_PAO}+S_{O})$	\lim_{O_PAO}
$K_{O_PAO}/(S_{O}+K_{O_PAO})$	\lim_{O_PAO}
$S_{O}/(K_{O_A}+S_{O})$	\lim_{O_A}
$S_{F}/(K_{F_H}+S_{F})$	\lim_{F_H}
$S_{F}/(K_{Fe_H}+S_{F})$	\lim_{Fe_H}
$S_{F}/(S_{F}+S_{A})$	cons_F
$S_{A}/(K_{A_H}+S_{A})$	\lim_{A_H}
$S_{A}/(S_{A}+S_{F})$	cons_A
$S_{A}/(K_{A_PAO}+S_{A})$	\lim_{A_PAO}
$S_{NH4}/(K_{NH4_H}+S_{NH4})$	\lim_{NH4_H}
$S_{NH4}/(S_{NH4}+K_{NH4_PAO})$	\lim_{NH4_PAO}
$S_{NH4}/(S_{NH4}+K_{NH4_A})$	\lim_{NH4_A}
$S_{NO3}/(K_{NO3_hyd}+S_{NO3})$	\lim_{NO3_hyd}

$K_{NO3_hyd}/(K_{NO3_hyd}+S_{NO3})$	inh_NO3_hyd
$S_{NO3}/(K_{NO3_H}+S_{NO3})$	lim_NO3_H
$K_{NO3_H}/(K_{NO3_H}+S_{NO3})$	inh_NO3_H
$S_{NO3}/(K_{NO3_PAO}+S_{NO3})$	lim_NO3_PAO
$S_{PO4}/(K_{P_H}+S_{PO4})$	lim_P_H
$S_{PO4}/(K_{PSt_PAO}+S_{PO4})$	lim_PS_PAO
$S_{PO4}/(K_{P_PAO}+S_{PO4})$	lim_P_PAO
$S_{PO4}/(K_{P_A}+S_{PO4})$	lim_P_A
$(X_S/X_H)/(K_{Xcod_hyd}+X_S/X_H)$	lim_sur_hyd
$(X_{PP}/X_{PAO})/(K_{PP_PAO}+X_{PP}/X_{PAO})$	lim_stor_PP
$(X_{PHA}/X_{PAO})/(K_{PHA_PAO}+X_{PHA}/X_{PAO})$	lim_stor_PHA
$(K_{max_PAO}-X_{PP}/X_{PAO})/(K_{IPP_PAO}+K_{max_PAO}-X_{PP}/X_{PAO})$	lim_stor_PP_max

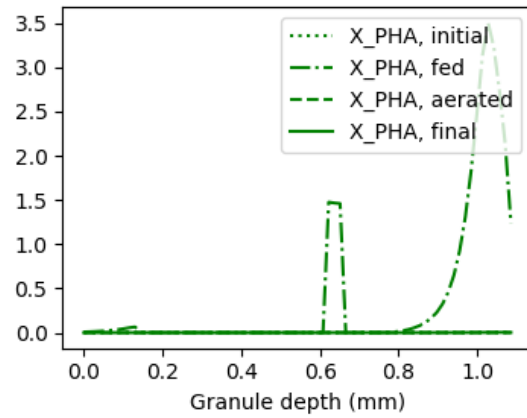
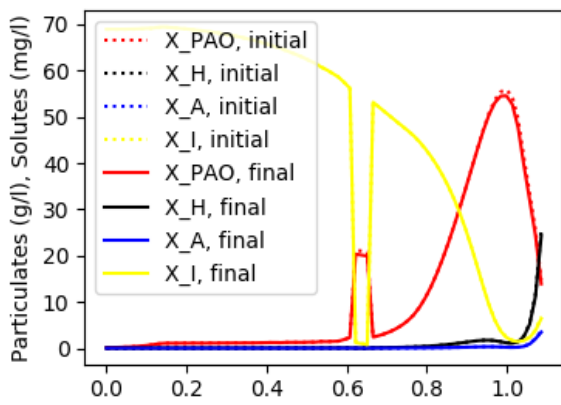
Kinetic parameters:

K_hyd	3	[1/d]
q_fe	3	[1/d]
q_PHA	3	[1/d]
q_PP	1.5	[1/d]
eta_NO3_hyd	0.6	
eta_fe_hyd	0.4	
eta_NO3_H	0.8	
eta_NO3_PAO	0.6	
K_O_hyd	0.2	[g/m ³]
K_Xcod_hyd	0.1	[g/g]
K_NO3_hyd	0.5	[g/m ³]
K_O_H	0.2	[g/m ³]
K_F_H	4	[g/m ³]
K_NH4_H	0.05	[g/m ³]
K_P_H	0.01	[g/m ³]
K_A_H	4	[g/m ³]
K_NO3_H	0.5	[g/m ³]
K_Fe_H	4	[g/m ³]
K_O_PAO	0.2	[g/m ³]
K_NO3_PAO	0.5	[g/m ³]
K_A_PAO	4	[g/m ³]
K_NH4_PAO	0.05	[g/m ³]
K_PSt_PAO	0.2	[g/m ³]
K_P_PAO	0.01	[g/m ³]
K_PP_PAO	0.01	[g/g]
K_IPP_PAO	0.02	[g/g]
K_max_PAO	0.34	[g/g]
K_PHA_PAO	0.01	[g/g]
K_O_A	0.5	[g/m ³]
K_NH4_A	1	[g/m ³]
K_P_A	0.01	[g/m ³]

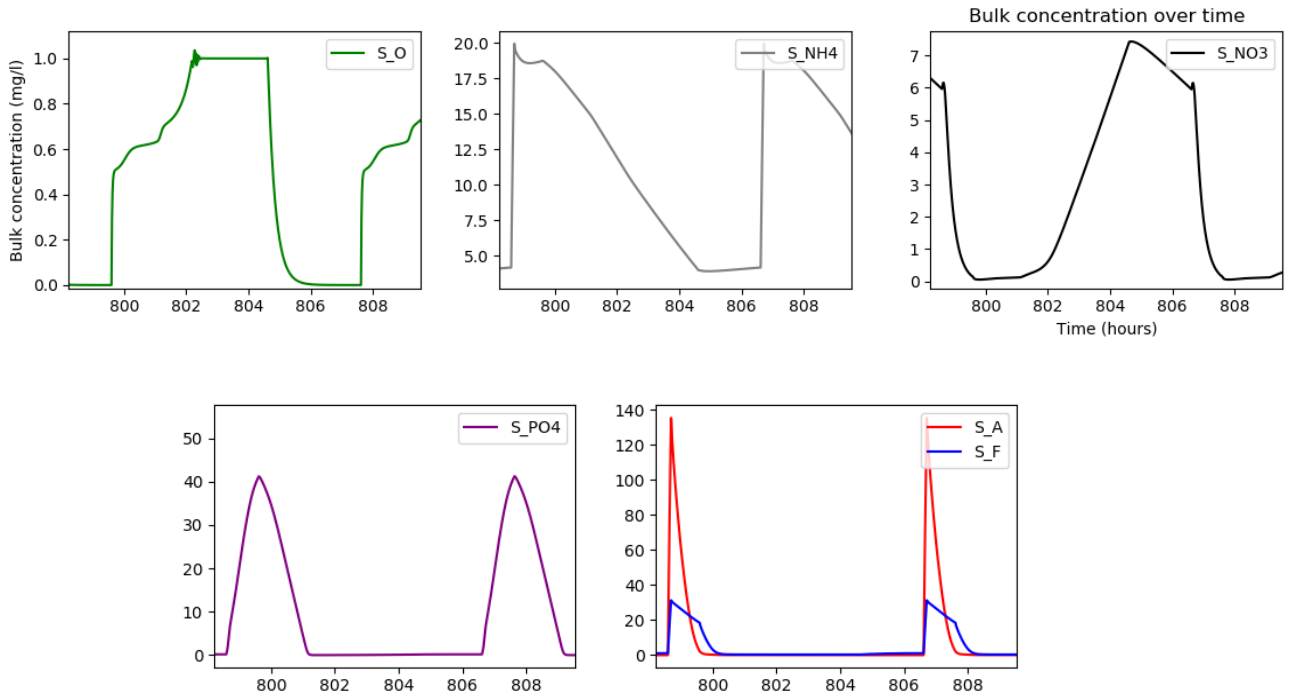
	Diffusion	Density	Decay rate / lysis rate	Maximum growth rate
	D	rho	b	mu
	[m ² /s]	[g/L]	[1/d]	[1/d]
S_O	2.31E-09	0	0	0
S_F	5.00E-10	0	0	0
S_A	1.11E-09	0	0	0
S_NH4	1.97E-09	0	0	0
S_N2	1.00E-09	0	0	0
S_NO3	1.85E-09	0	0	0
S_PO4	1.27E-09	0	0	0
X_I	0.00E+00	20	0	0
X_S	0.00E+00	80	0	0
X_H	0.00E+00	80	0.4	6
X_PAO	0.00E+00	80	0.05	1
X_PP	0.00E+00	20	0.05	0
X_PHA	0.00E+00	20	0.05	0
X_A	0.00E+00	80	0.15	1

Appendix B: Single granule model

Steady state granule profile (without corrections for breaks in the graph)

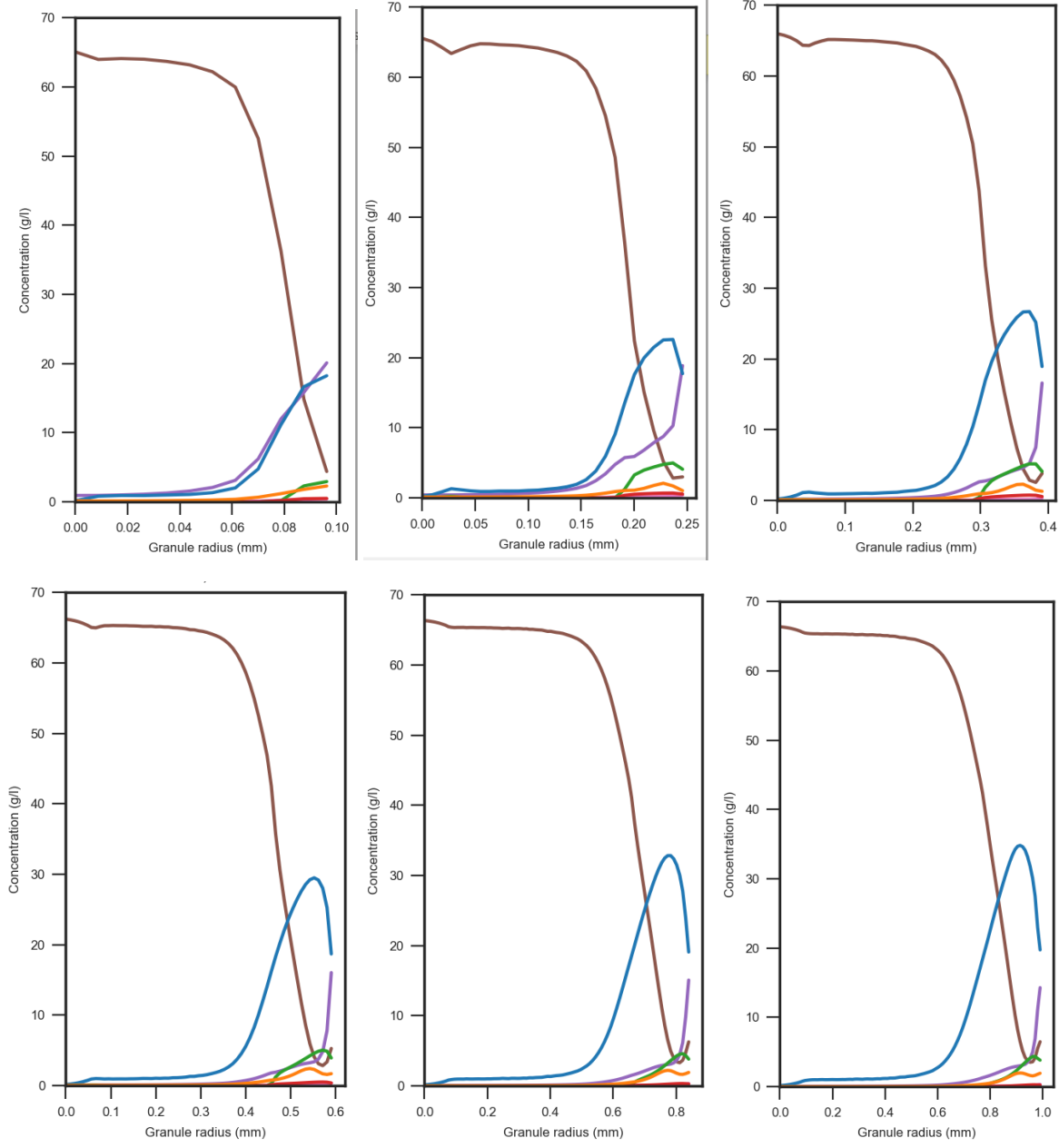


Steady state bulk concentrations over two cycles

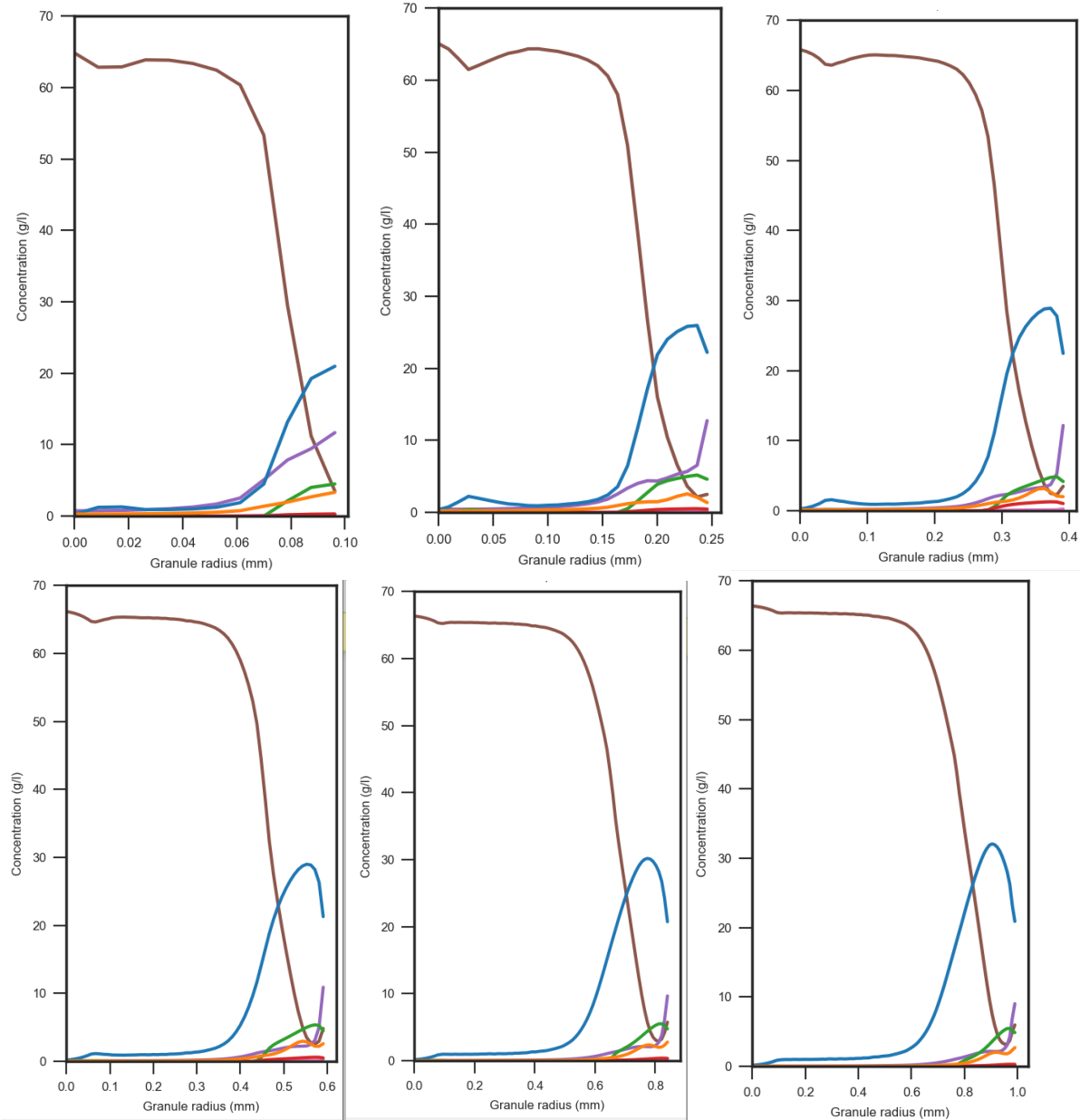


Appendix C: Concentration profiles over granules, end of feeding

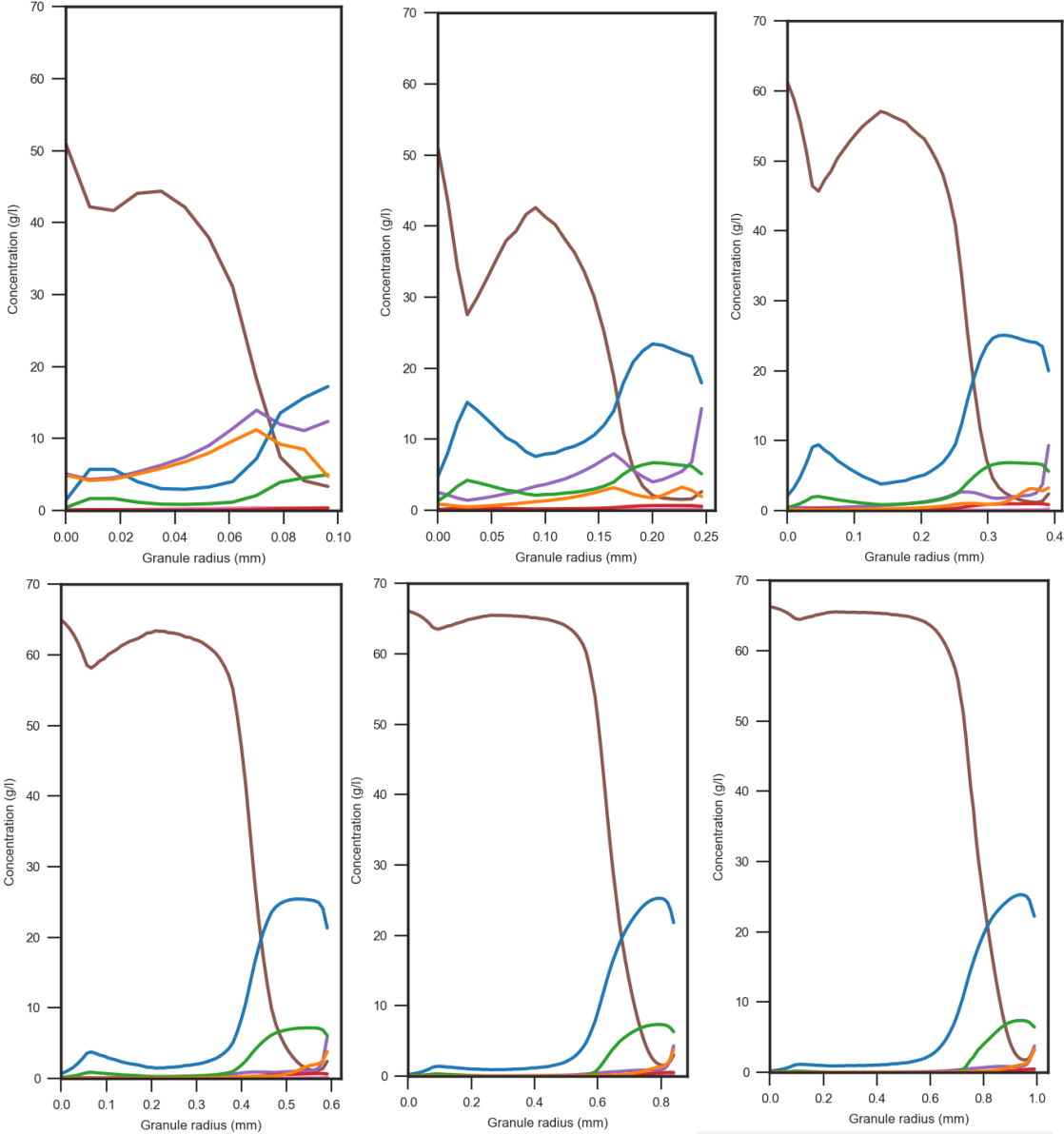
Concentration profiles of all granules for 50 mg/l acetate run (at the end of the feeding phase)



Concentration profiles of all granules for 100 mg/l acetate run (at the end of the feeding phase)

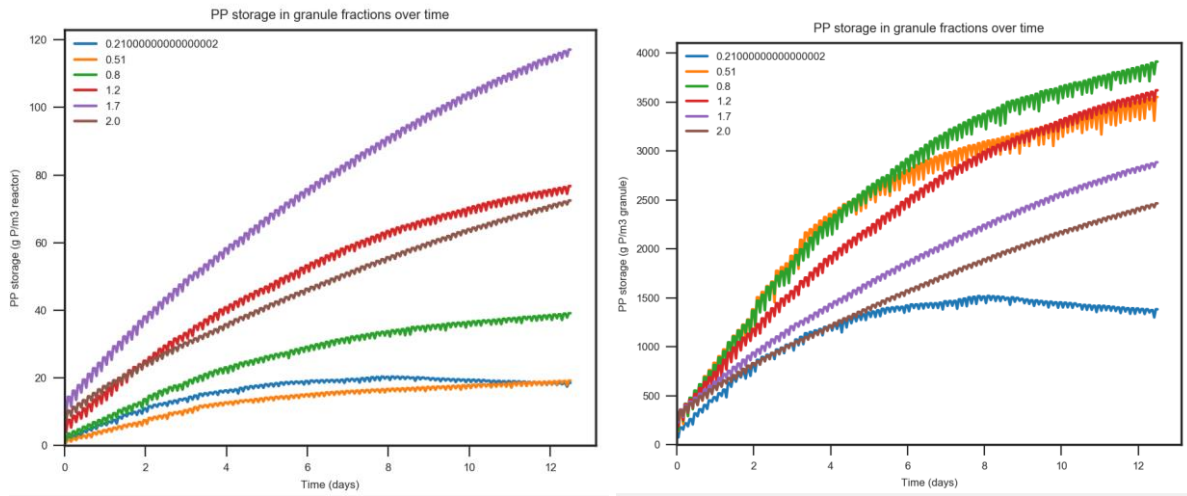


Concentration profiles of all granules for 150 mg/l acetate run (at the end of the feeding phase)

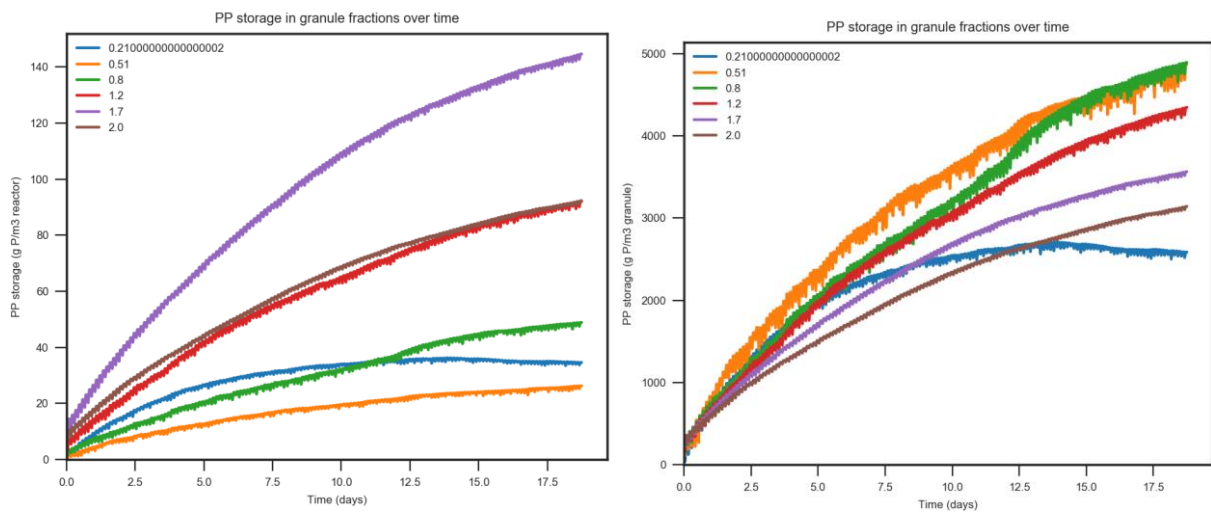


Appendix D: PP storage per granule size over time

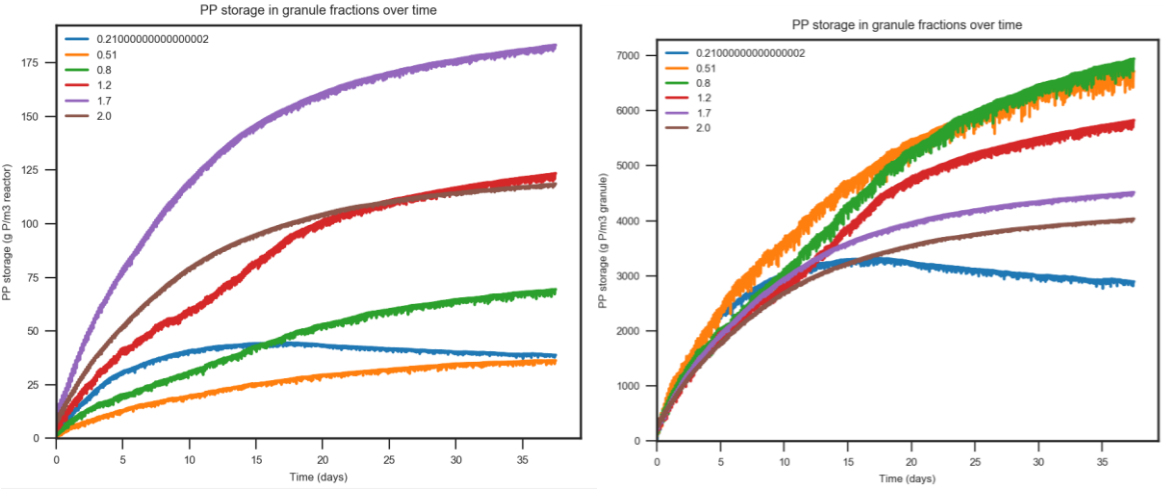
PP storage for the 50 mg/l acetate run over time (per granule volume, left, and per reactor volume, right)



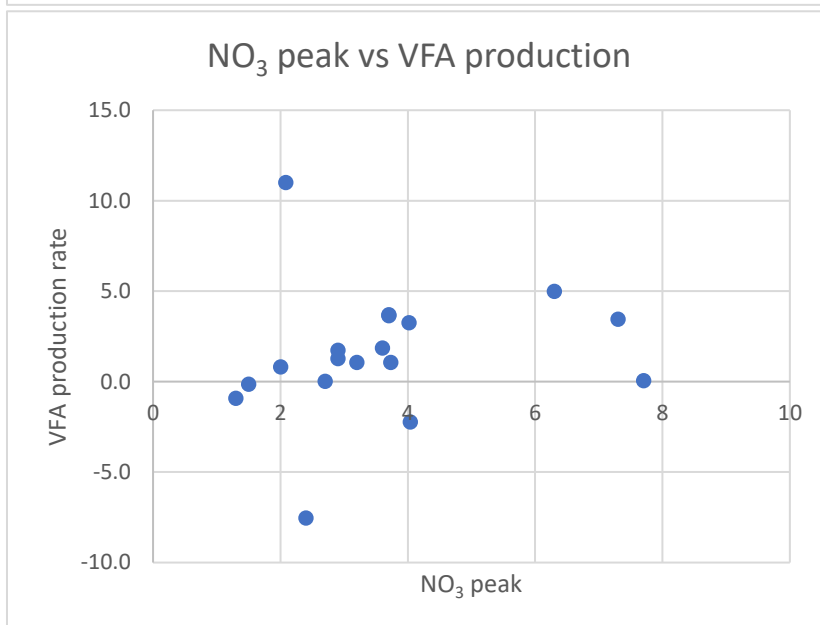
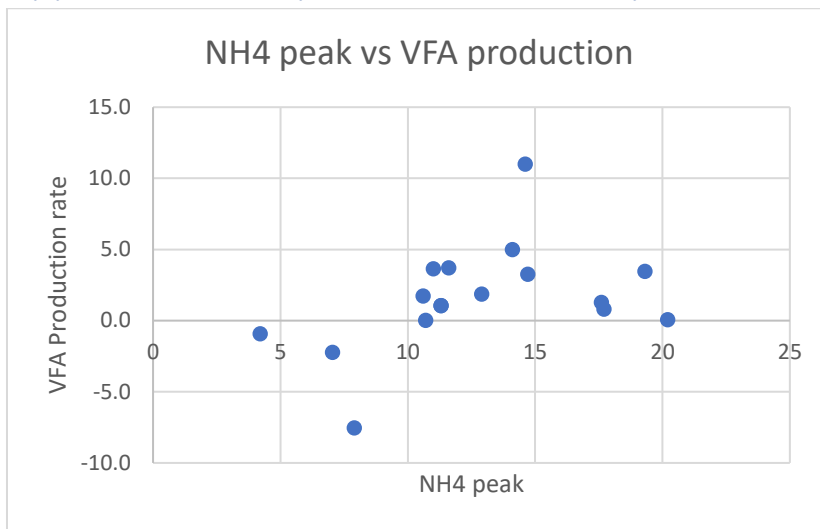
PP storage for the 100 mg/l acetate run over time (per granule volume, left, and per reactor volume, right)

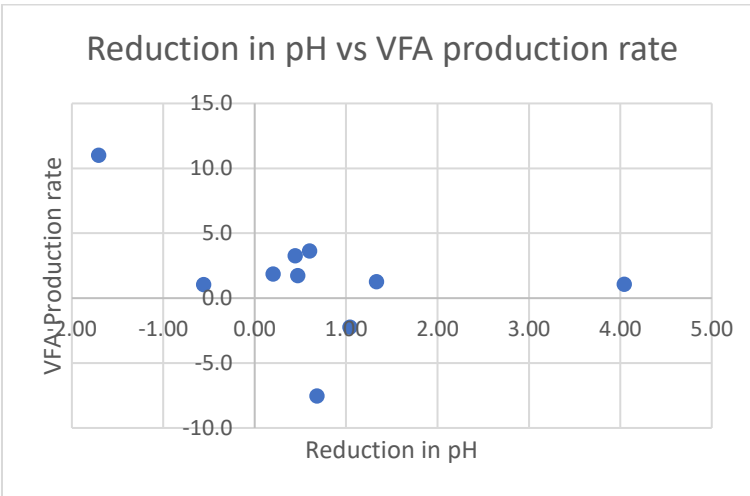
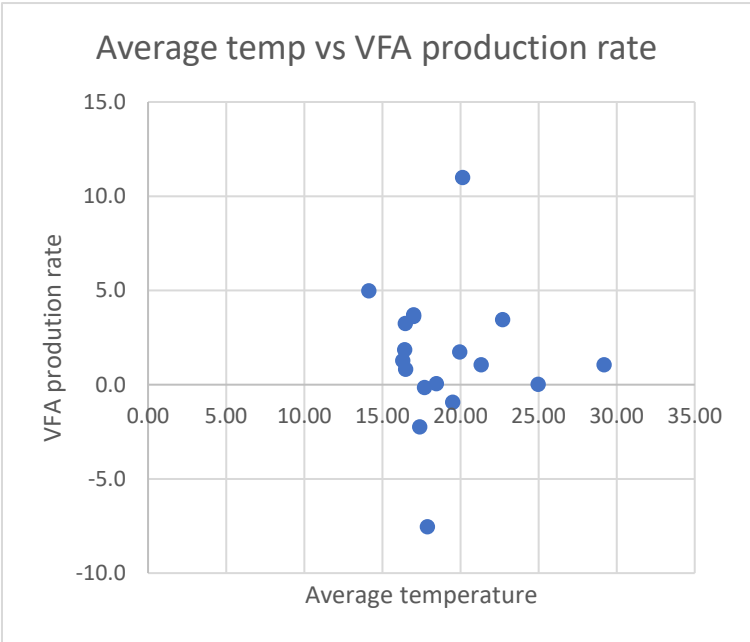
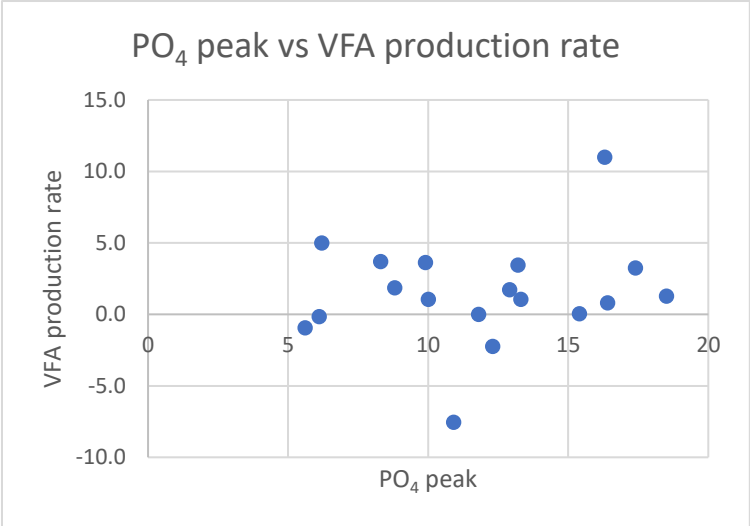


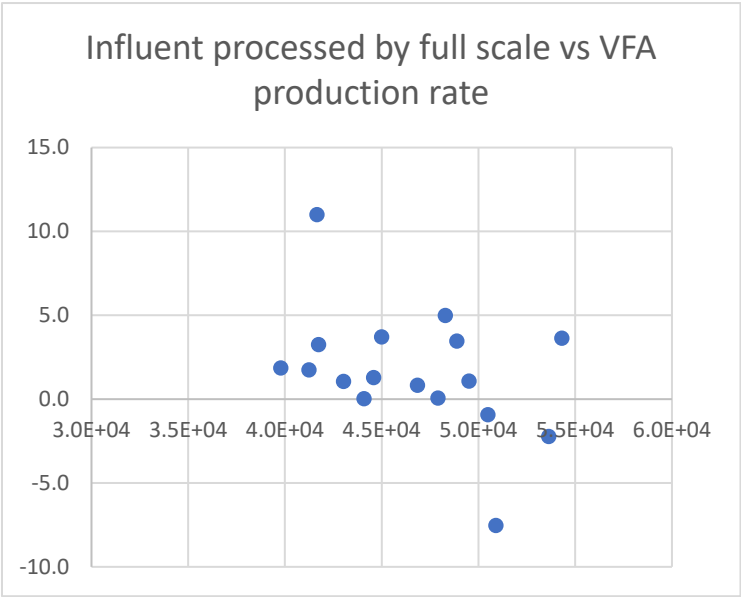
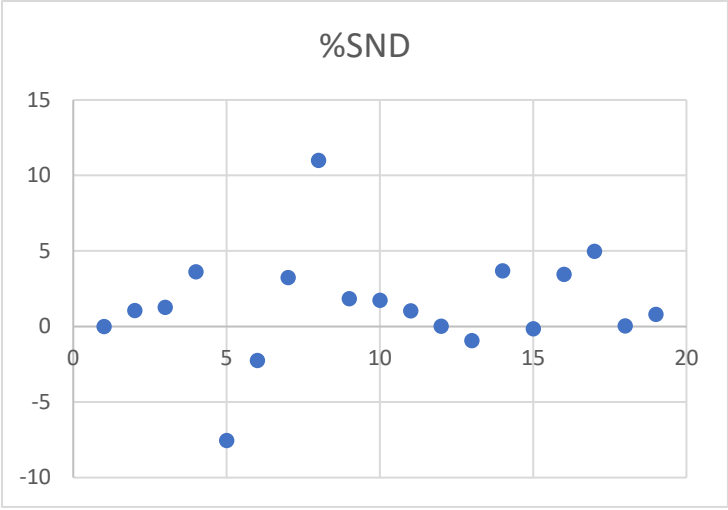
PP storage for the 150 mg/l acetate run over time (per granule volume, left, and per reactor volume, right)



Appendix E: VFA production rate vs. peak concentrations in PNU

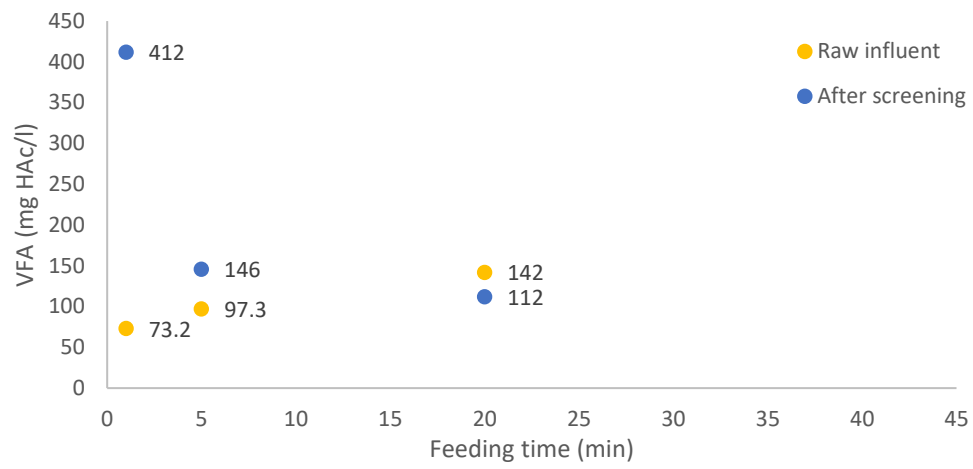




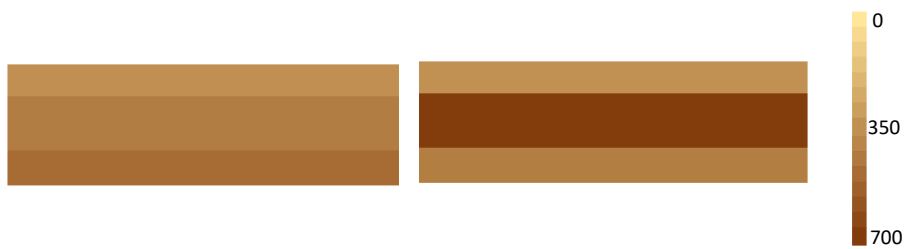


Appendix F: Additional sand trap measurements

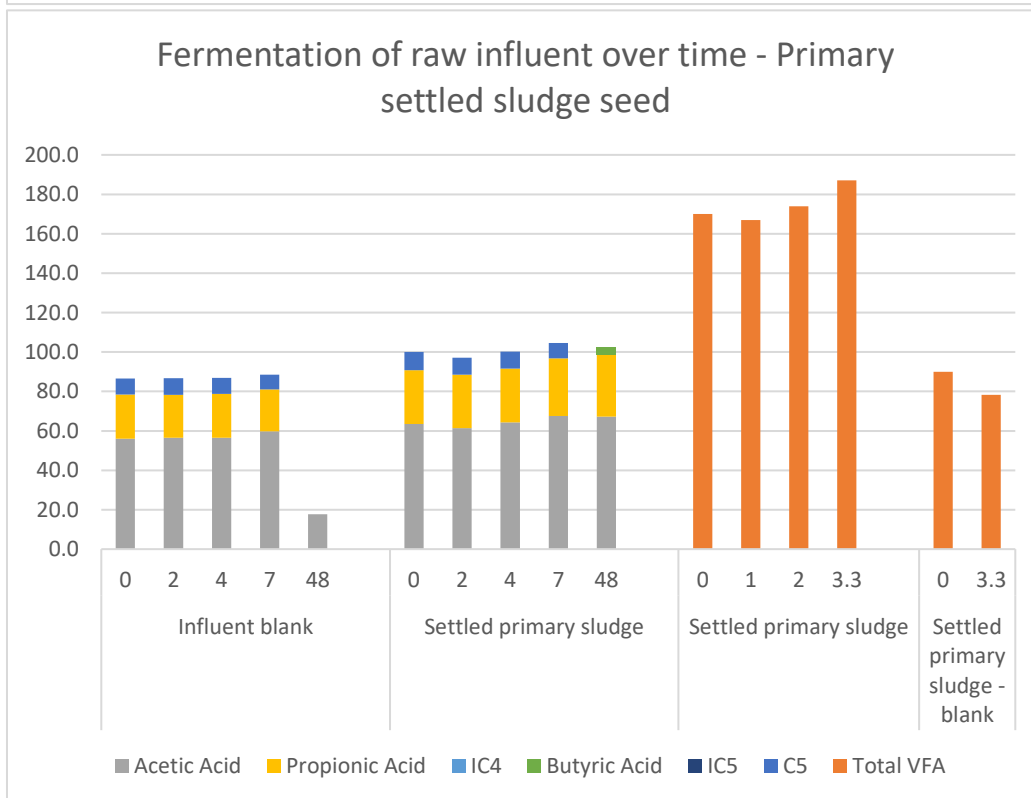
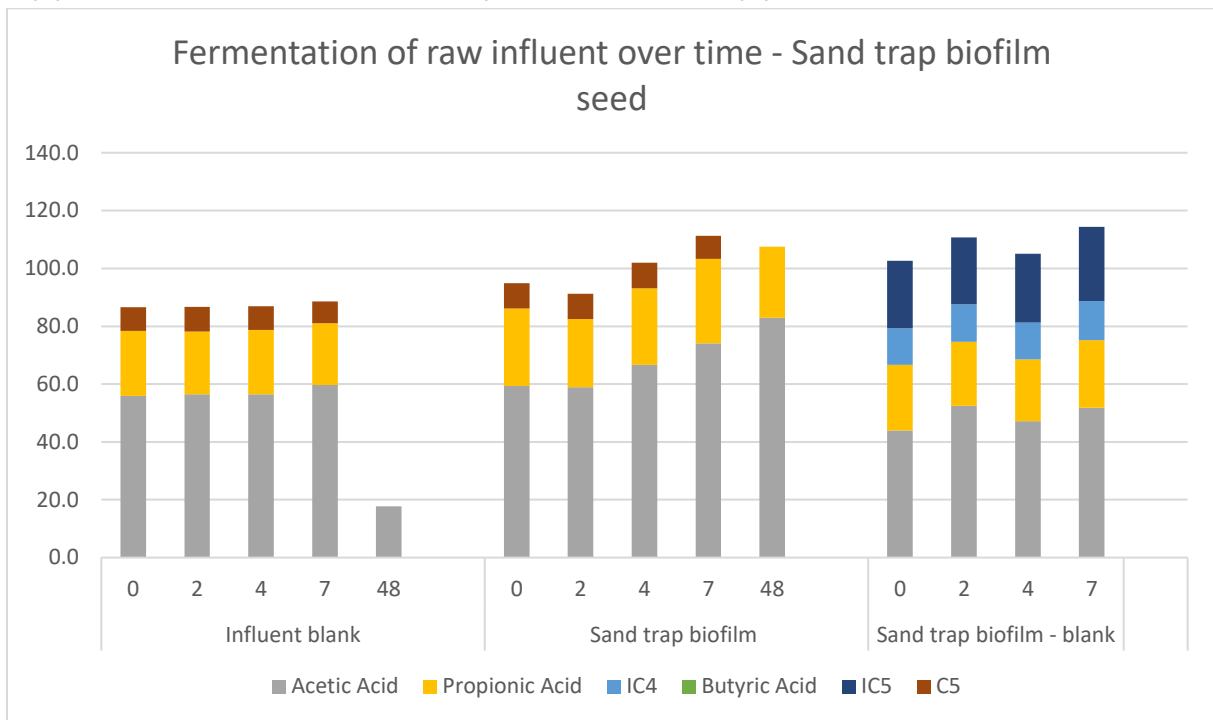
Repeated measurements on influent at two different points in the primary treatment over a PNU feeding phase

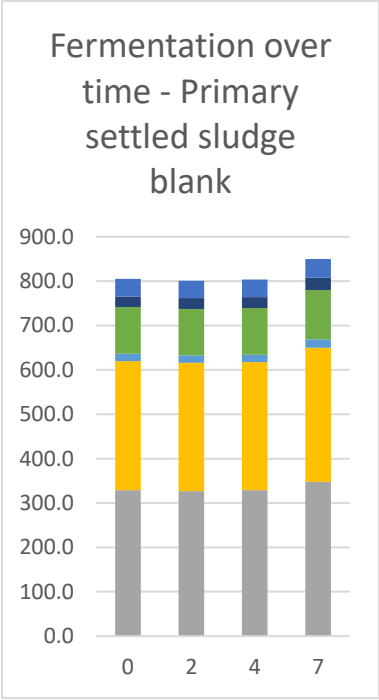
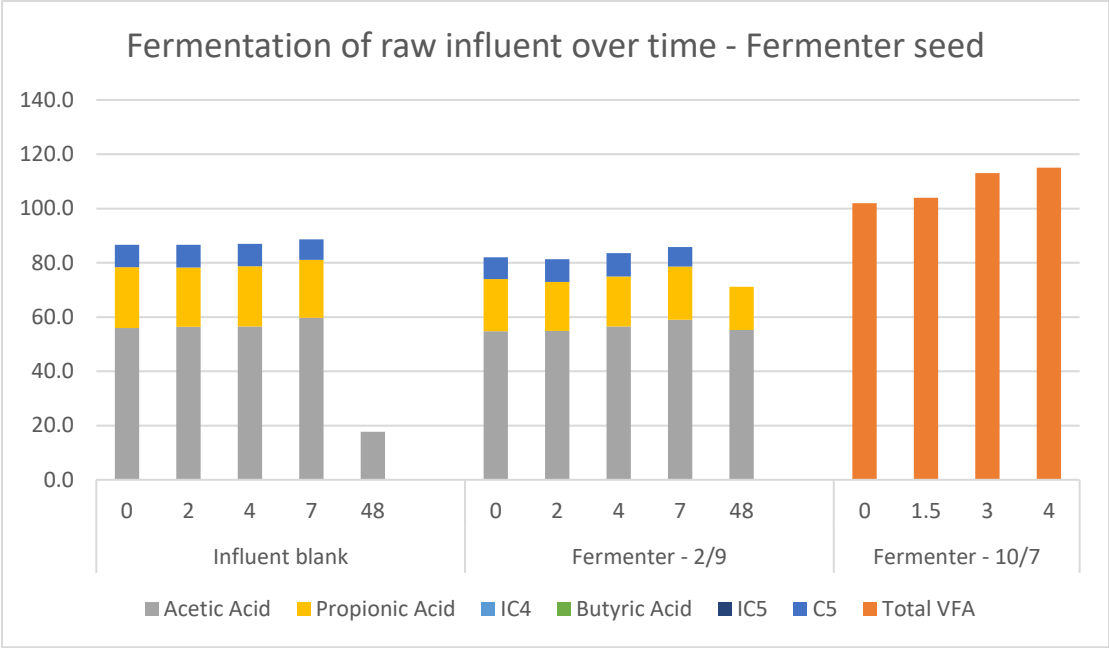


VFA measurements at two sample points over the depth of the sand trap at the end of the PNU cycle

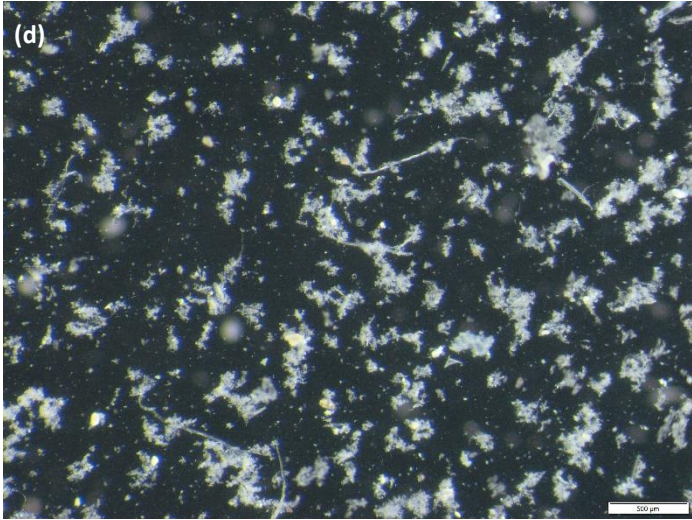
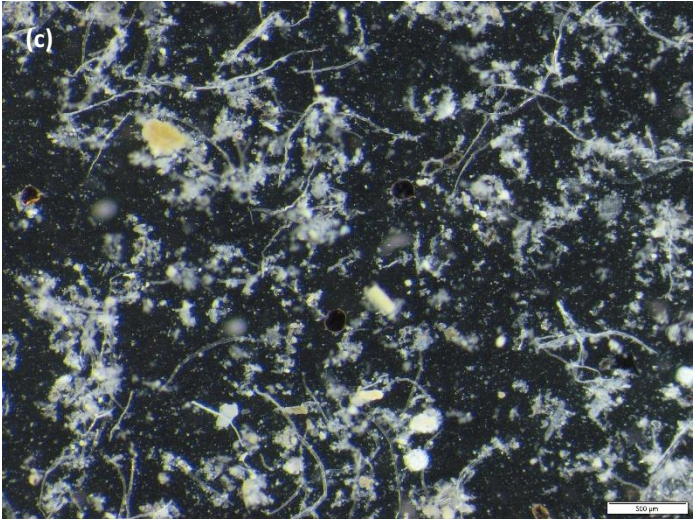
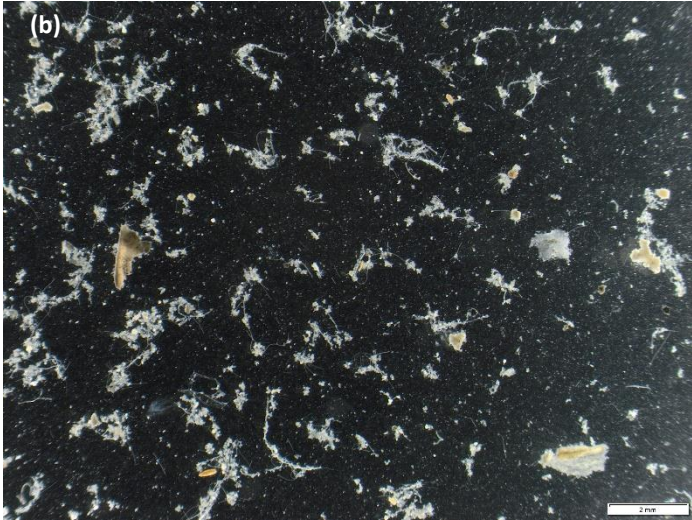
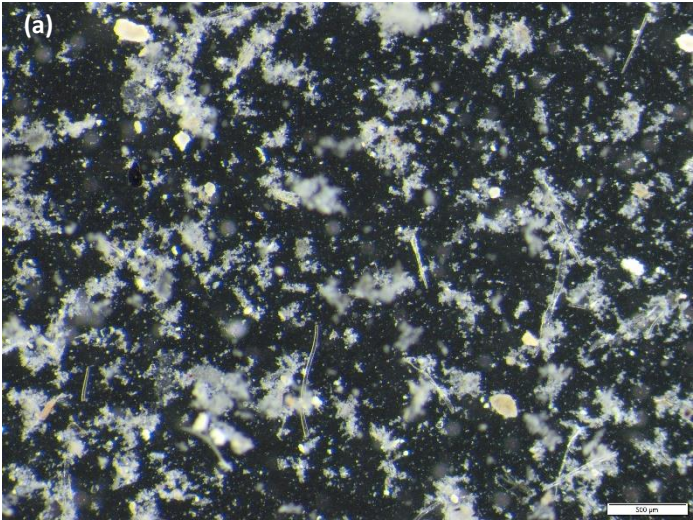


Appendix G: Biomass activity and microscopy

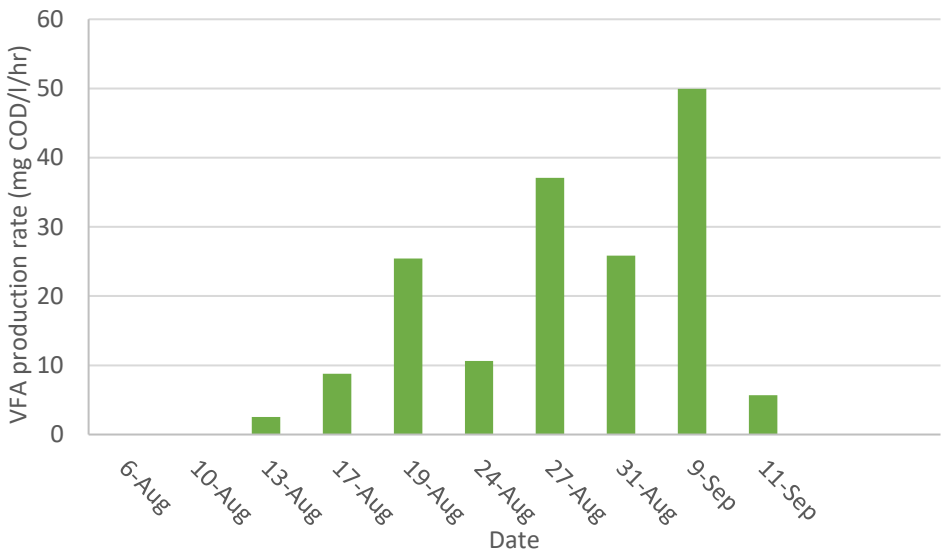




Microscopy of biomass from the sand trap and fermenter (a) fermenter sludge, (b) biofilm from sand trap walls, (c) settled sludge from sand trap, (d) scum layer from fermenter

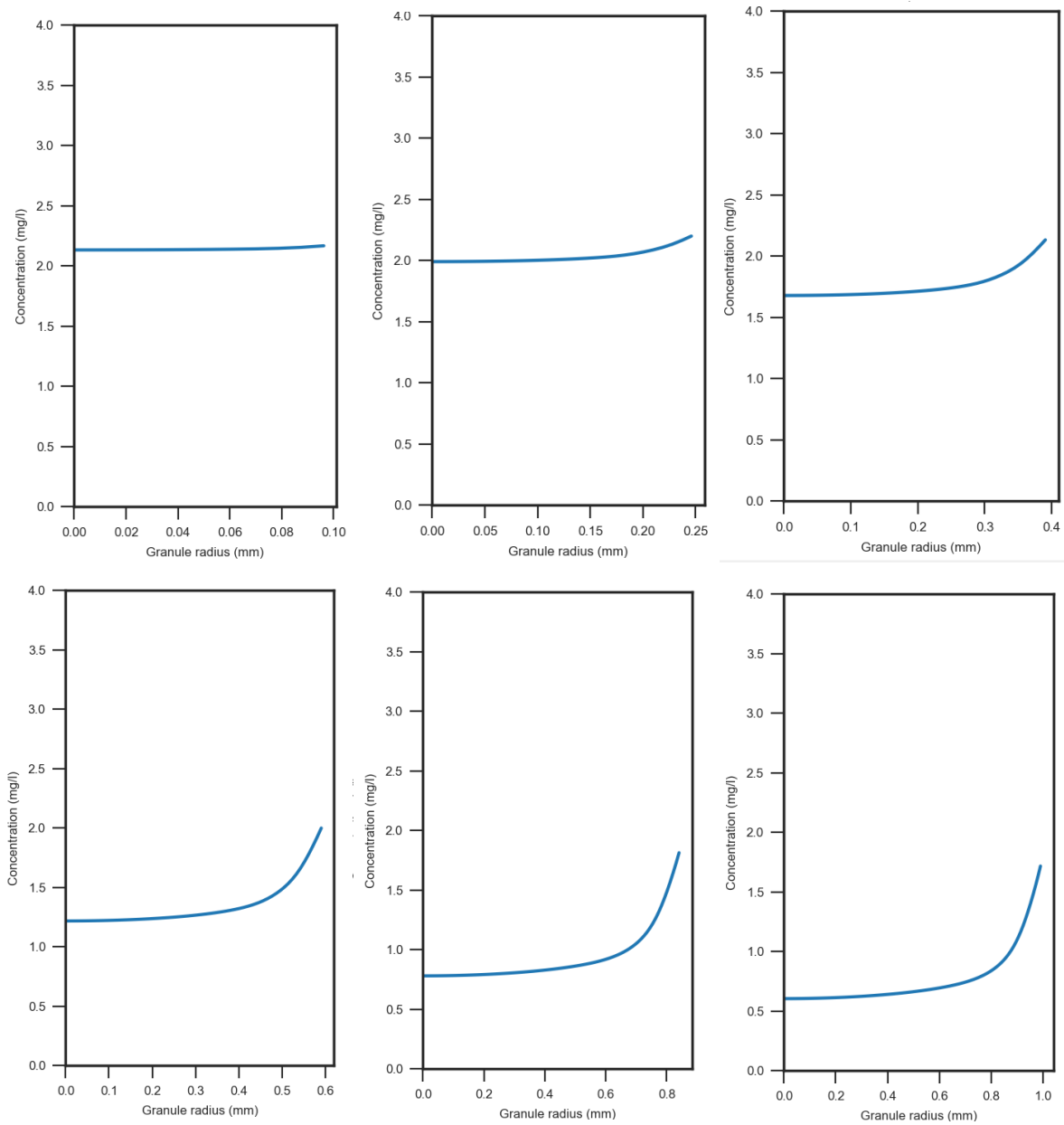


Appendix H: VFA production rates in the sand trap over time

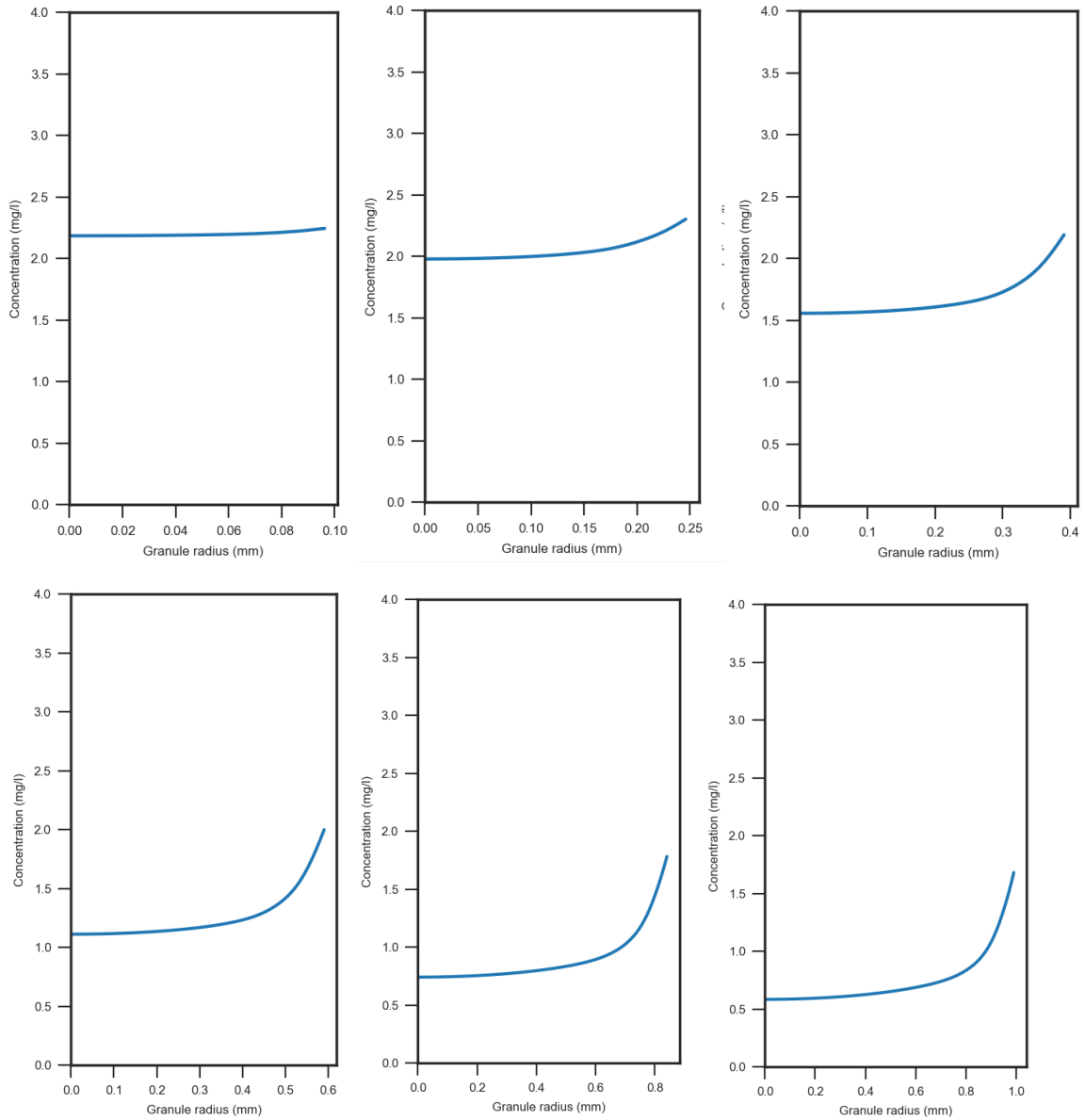


Appendix I: Oxygen penetration over different granule sizes

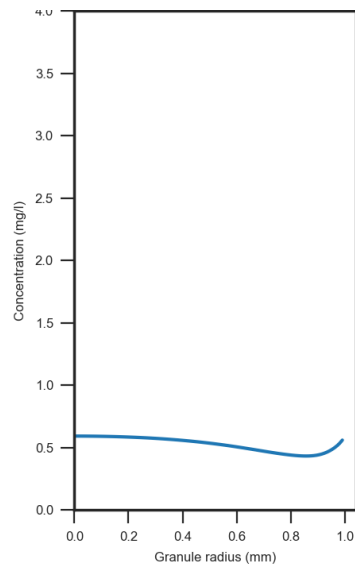
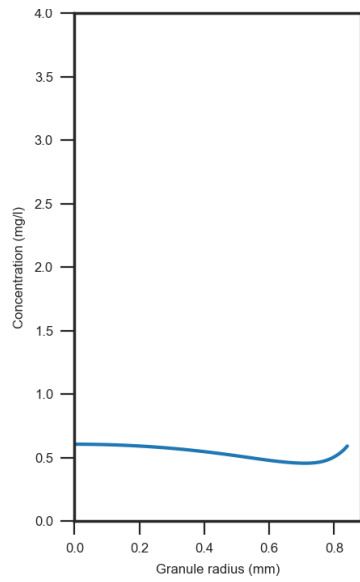
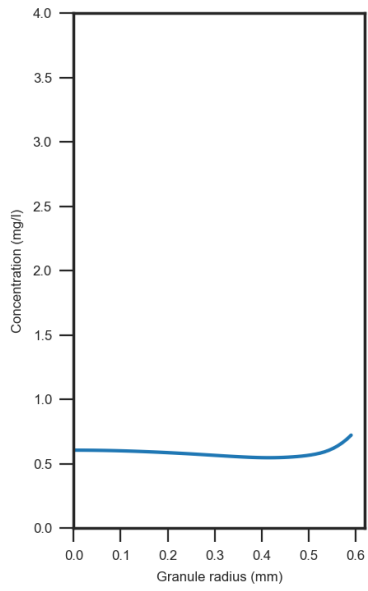
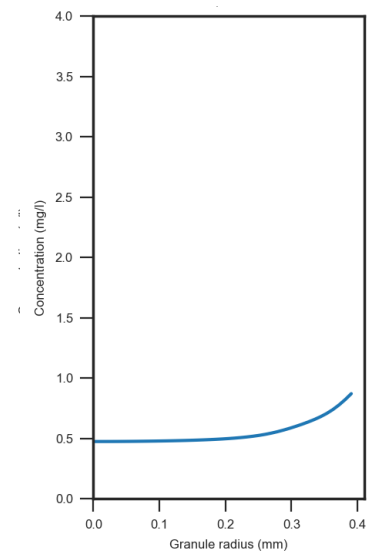
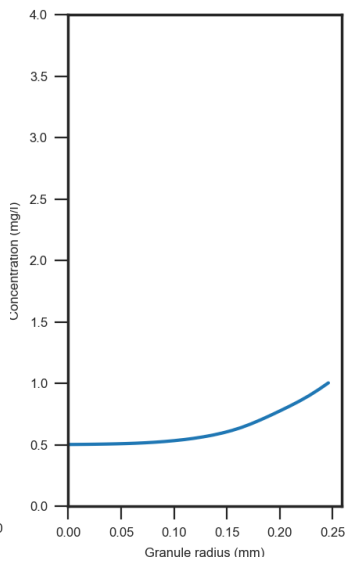
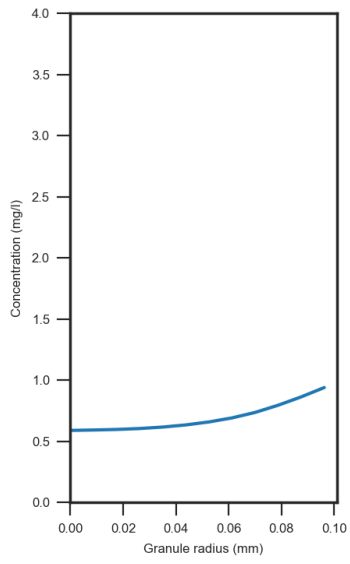
Oxygen penetration over granules over different sizes for 50 mg/l acetate:



Oxygen penetration over granules over different sizes for 100 mg/l acetate:



Oxygen penetration over granules over different sizes for 150 mg/l acetate:



Appendix J: Substrate front vs. sludge bed expansion

